

CZECH TECHNICAL UNIVERSITY IN PRAGUE
ELECTROTECHNICAL FACULTY

LULEA TECHNICAL UNIVERSITY IN SWEDEN
FACULTY OF SPACE SCIENCE AND TECHNOLOGY



DIPLOMA THESIS

Helicopter in virtual space

Prague, 2008

Author: Michal Hoč

Declaration

I, Michal Hoč, honestly declare, that I have worked out my diploma thesis individually and all resources (literature, projects, SW etc.) that I have used I have stated in the attached list.

In Prague, date _____

signature

Acknowledgements

I would like to thank my supervisors František Vaněk and Thomas Gustafsson for their priceless advises during development of the Thesis, their patience and time.

Abstract

This work explores two different approaches in the helicopter system (HUMUSOFT CE-150) identification. The obtained mathematical model of the helicopter is used for the control synthesis of PD, PID, LQG and MPC. The performances of controllers are mutually compared through the step responses with the standard amplitudes. The real time interconnection of the virtual reality helicopter model with the real helicopter system enhances the flight impression. The robustness of the control design is checked by the reaction of the system during the flight to the outside disturbances.

MASTER THESIS ASSIGNMENT

Student: Michal H o ě
Field of Study: Cybernetics and Measurement - SpaceMaster
Thesis Title: Helicopter in virtual space

Thesis Guidelines:

1. Study the helicopter model Humusoft (or Spel).
2. Identify the system in two dimensions, set up MATLAB scripts for quick check of the parameters.
3. Design set of PID regulators for 2D control.
4. Design regulators by the means of modern methods of control synthesis (LQ, LQG etc.) and compare the responses with PID regulators performance.
5. Find the effective representation of the 3D landscape profile in MATLAB.
6. Design the system, which controls the physical model and the scanned data is fed back to the virtual landscape in real time. The goal is to achieve the minimal height above the terrain.
7. Use VR – toolbox to simulate the position and the movements of the helicopter in the virtual environment.
8. Test the system behavior when exposed to typical atmospheric irregularities: wind gusts, uneven up thrust due to warm wind stream etc.

Bibliography:

Supervisor:

Contents

List of Figures	xii
List of Tables	xiii
List of Symbols	xv
1 Introduction	1
2 System Analysis	3
2.1 Inputs and outputs	3
2.2 Subsystem description	3
2.2.1 Working point as a static equilibrium	4
2.2.2 Motors	6
2.2.3 Propellers	7
2.2.4 Mechanical parts	8
2.2.5 The subsystem interconnection	8
2.2.6 The working point selection	9
2.3 Linearization	10
2.3.1 The linearization of the state equations	10
2.4 State space model	12
2.4.1 State space matrices	12
2.4.2 From the state space description to the transfer matrix	14
3 Identification methods	17
3.1 Static characteristics	17
3.1.1 Strategies for static experiments	17
3.1.2 Equilibria	18
3.1.3 Steady state spinning rate of motors	18

3.2	Dynamic characteristics	19
3.2.1	Strategies for the evaluation of dynamic responses	19
3.2.2	The first algorithm for step response evaluation	20
3.2.3	The limits of the first algorithm	23
3.2.4	The second algorithm for step response evaluation	24
3.2.5	The limits of the second algorithm	25
3.2.6	The state space model evaluation	26
4	System Identification	27
4.1	Static characteristics	27
4.1.1	Ranges and the conversion of units	27
4.1.2	Static equilibria characteristics	28
4.1.3	Steady state spinning rate of motors	29
4.1.4	Initial conditions	33
4.2	Dynamic characteristics	34
4.2.1	The input signal	35
4.2.2	Evaluation of step responses with 'holding'	37
4.2.3	Evaluation of free step responses	38
4.2.4	The identification strategy modification	39
4.2.5	The direct identification of the motors dynamics	40
4.2.6	The identification of the first working point	42
4.2.7	The identification of the second working point	43
4.2.8	The identification of the third working point	44
5	Control Synthesis	45
5.1	Classical Control Theory	45
5.1.1	Decoupling	46
5.1.2	Frequency methods for PD control design	48
5.1.3	Frequency methods for PID control design	52
5.1.4	Root locus methods for PID control design	55
5.2	Modern Control Theory	58
5.2.1	The discretization of the continuous system	58
5.2.2	Kalman filter design	59
5.2.3	LQG control design	62
5.2.4	Model Predictive Control (MPC) design	65

6	Virtual Reality	69
6.1	The design of VR objects	69
6.2	Simulation	70
7	Conclusion	71
	Literature	73
A	The content of attached CD	I

List of Figures

1.1	The helicopter CE 150	1
2.1	The interconnection of all subsystems of the helicopter	4
2.2	Tilted lever	4
2.3	Servo motor - illustrative figure	6
2.4	Propeller - illustrative figure	7
2.5	The state space model	13
2.6	The modified state space model for the zero initial conditions	14
2.7	The impulse and step response of the system $G(s)$	15
3.1	Motors dynamics identification strategy	19
3.2	Identification strategy for the rest of working points	20
3.3	The dynamics separation identification algorithm	22
3.4	Short time step response experiment - wrong results	23
3.5	$z(t)$ function	25
4.1	Static characteristics - equilibria measurement	28
4.2	Schematics for the slotted optosensor interconnection	29
4.3	The settings of the experiment	29
4.4	The steady state spinning rate of the main motor	30
4.5	The steady state spinning rate of the tail motor	31
4.6	The mutual steady state spinning rate characteristics	32
4.7	Input signal for the measurement of dynamic responses	35
4.8	The Simulink scheme for the system identification - holding	36
4.9	The Simulink scheme for the system identification - Azimuth	36
4.10	The Simulink scheme for the system identification - Elevation	36
4.11	The transient response around the vertical axis of rotation, red - model	37
4.12	Tail motor identification cyan - holding, blue - free, red - model	38

4.13	Main motor step response, red - model	41
4.14	Tail motor step response, red - model	41
4.15	Step responses of the system and model(red)	42
4.16	Step responses of the system and model(red)	43
4.17	Step responses of the system and model(red)	44
5.1	The feedback control scheme	45
5.2	Pure PD controller design - frequency methods	49
5.3	Lead compensated PD controller design - frequency methods	50
5.4	The comparison of the system and model step responses	51
5.5	Lead compensated PID controller design - frequency methods	52
5.6	The comparison of the system and model step responses	53
5.7	The comparison of the system and model step responses - coupling	54
5.8	The root locus of the S_{HM}	55
5.9	The root locus of the S_{VT}	56
5.10	The comparison of the system and model step responses	57
5.11	The Kalman filter Simulink scheme	60
5.12	The comparison of the estimated states (blue) and model(red)	61
5.13	The Simulink scheme for the LQG	63
5.14	The comparison of the system and model step responses	64
5.15	The Simulink scheme for the MPC	67
5.16	The comparison of the system and model step responses	68
6.1	Virtual landscape and helicopter	69
6.2	The interconnection of the VR with the Simulink scheme	70
6.3	The internal interconnection of the signal expander	70

List of Tables

4.1	The input and output vector ranges and conversion constants	27
4.2	Input $u(0)$ and state $x(0)$ vectors for the working point 1	33
4.3	Input $u(0)$ and state $x(0)$ vectors for the working point 2	33
4.4	Input $u(0)$ and state $x(0)$ vectors for the working point 3	33
4.5	The F_{VT} identification of working point 2	38
4.6	The G_{VT} identification of working point 2	39
4.7	The dynamics of motors	41

Notation

List of Symbols

ψ	elevation angle measured from the local horizontal - clockwise negative
ϕ	azimuth angle measured from the central position - clockwise positive
U_M	the input voltage applied on the main motor
U_T	the input voltage applied on the tail motor
U_B	the input voltage applied on the motor shifting the mass point
M	torque
ω	the angular speed - the state variable of the helicopter
J	the moment of inertia
B	the linear friction
k_M	proportionality constant of main motor
k_T	proportionality constant of tail motor
k_2	proportionality constant of propeller
k_1	proportionality constant of propeller
M_g	moment caused by the gravity force acting on the helicopter
l	effective distance
F_g	gravity force
k_B	constant transfer ratio
∂	represents small perturbations from the equilibrium value
p_M	pole characterising main motor dynamics
p_T	pole characterising tail motor dynamics
p_V	pole characterising dynamics of the system around the vertical axis of rotation
p_H	pole characterising dynamics of the system around the horizontal axis of rotation
ρ	constant of the propeller in an equilibrium
x	state vector of the system
$x(0)$	state vector defining equilibrium of the system
X	Laplace transformation of a state vector of the system
u	input vector of the system
U	Laplace transformation of an input vector of the system
y	output vector of the system

Y	Laplace transformation of an output vector of the system
s	complex variable
G	the transfer matrix of the system
κ	gain of the transfer matrix G of the system
$u(0)$	the necessary constant input vector to keep the system in equilibrium
$y(0)$	the constant output vector when the system is in equilibrium
T	the time of the experiment
T_s	the sampling time
F	the closed loop transfer matrix
H	the open loop transfer matrix
R	the transfer matrix of the controller
I	the unity matrix of the corresponding size

List of Subscripts

M	related to or generated by main motor (or propeller)
T	related to or generated by tail motor (or propeller)
H	acting around the horizontal axis of rotation
V	acting around the vertical axis of rotation
0	constant under steady state conditions

Chapter 1

Introduction

The main goal of this work is identification and control of a helicopter model CE 150 (further referred to as helicopter or system) provided by HUMUSOFT s.r.o.

<http://www.humusoft.cz/models/ce150.htm>.

The helicopter is connected to a personal computer and it is placed in laboratory K26 at the department of control engineering, electrotechnical faculty of Czech technical university in Prague.

The helicopter CE 150 corresponds to a classical propeller configuration and it is shown on the figure 1.1.

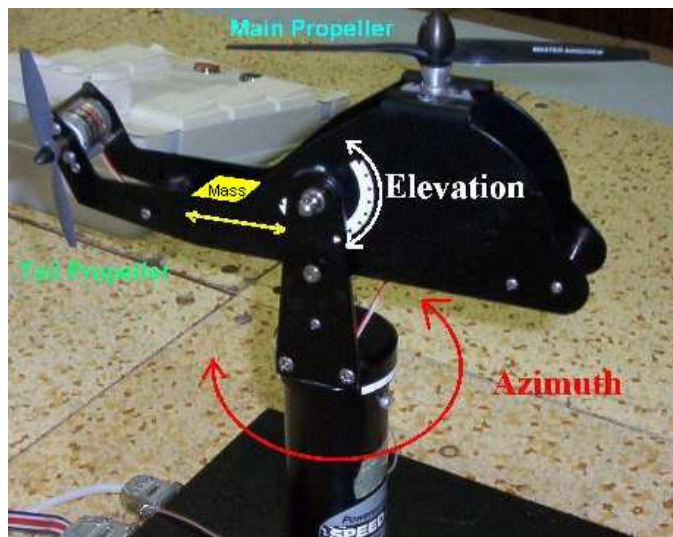


Figure 1.1: The helicopter CE 150

The helicopter is fixed to a rod therefore its motion is restricted to azimuth and

elevation angle.

At the steady state conditions the axis of the main propeller is parallel to local vertical and the axis of the tail propeller is parallel to local horizontal.

The steady state is defined by the center of mass of the helicopter. The center of mass is adjustable by the positioning of the cummulated weight in the lead box along the tail of the helicopter.

The angular velocities of the motors are adjustable by the input potential differences applied to the main and tail motors.

The conversion of the angular velocities of the motors to thrust force exerted by the propellers is non-linear. Thus the helicopter CE 150 from the point of view of theory of dynamical systems is non-linear Multiple Input Multiple Output (MIMO) system with two degrees of freedom (2 DOF).

To design a good control of the system it is necessary to know the mathematical model of the system. To obtain the mathematical model we start with the theoretical analysis of the system. The identification of the system is based on the mathematical model obtained. The quality of the mathematical model is checked by comparison of the transient responses of the system and model to standart signals - unit steps.

After the evaluation of all the unknown parameters we can proceed with the control synthesis. We base the control synthesis on the linearised model. We design a set of proportional-derivative PD and proportional-integrative-derivative PID controllers. During the analysis, identification and PD-PID control design we assume that the system and the data obtained is continuous in time.

The further control design requires discretising the mathematical model obtained. Before we design LQG controller (linear regulator with quadratic criterion assuming the Gaussian noise distribution) we will need to design a Kalman estimator of the state variables of the system that we are not able to measure.

We use the virtual reality (VR) toolbox in MATLAB for the virtual environment design. We will try to interconnect the virtual environment and the real system such that the information about the landscape is passed to the helicopter and the scanned data obtained from the helicopter CE 150 is fed back to the virtual environment in real time.

To ensure the minimal height of the flight above the known virtual terrain we will try to design MPC controller.

The robustness of the control design is checked by the exposing the helicopter model to the typical atmospheric irregularities such as wind gusts etc.

Chapter 2

System Analysis

This chapter sums up the main physical formulas of the individual subsystems, finds out continuous state-space representation of the system and derives the continuous transfer function of the system.

2.1 Inputs and outputs

The MIMO system of the helicopter has following input and output signals.

Symbol	Description
U_M	the input voltage applied on the main motor
U_T	the input voltage applied on the tail motor
U_B	the input voltage applied on the motor shifting the mass point
ψ	elevation angle measured from the local horizontal - clockwise negative
ϕ	azimuth angle measured from the central position - clockwise positive

2.2 Subsystem description

The helicopter as a system can be divided into three subsystems - motors, propellers and mechanical parts.

Motors convert the applied input voltages into angular speeds.

Propellers transform the angular speeds applied by motors into a force.

Mechanical parts of the helicopter are joints and the construction.

The logical line of the interconnection of all subsystems of the helicopter is represented on Fig. 2.1.

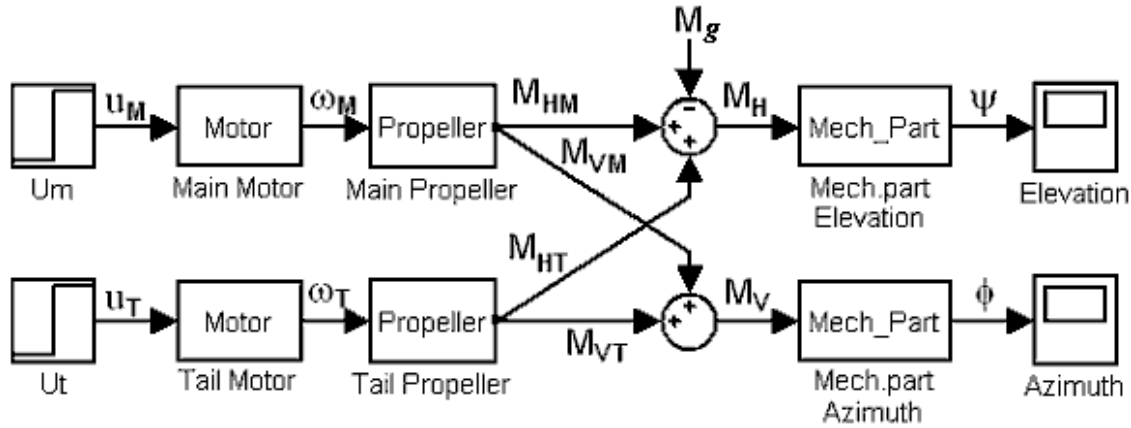


Figure 2.1: The interconnection of all subsystems of the helicopter

2.2.1 Working point as a static equilibrium

The helicopter is in the static equilibrium when its azimuth and elevation angles are constant and its motors are spinning at a constant angular velocities.

The input signals necessary to set the helicopter in the equilibrium state are defining its Working Point (WP).

The Fig. 2.2 shows the helicopter, simplified by a lever, tilted from its static equilibrium position.

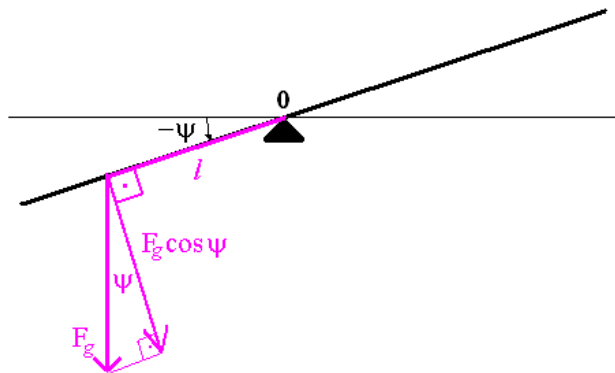


Figure 2.2: Tilted lever

We assume that the center of gravity is accumulated at effective distance l from the suspension point. The moment M_g caused by the gravity force acting on the helicopter is:

$$M_g = l \cdot F_g \cdot \cos \psi$$

M_g moment caused by the gravity force acting on the helicopter
 l effective distance
 F_g gravity force

We assume that for small elevation angle ψ the M_g is directly proportional to the actual position of the mass point of the helicopter which linearly depends on the U_B voltage.

$$M_g = k_B \cdot U_B \tag{2.1}$$

k_B constant transfer ratio $k_B \in \mathbb{R}$

We will examine the static equilibrium and the working point closer at the end of this section.

2.2.2 Motors

Motor consists of a stator and a rotor Fig. 2.3. The stator is steady whereas the rotor spins according to the applied voltage.



Figure 2.3: Servo motor - illustrative figure

We characterize the rotor as a mass with certain moment of inertia J spinning at angular frequency ω overcoming an internal friction B . If we neglect the induction of the rotor windings we can assume that the torque generated by the motor linearly depends on the input voltage applied to the motor.

$$k_M \cdot U_M = J_M \cdot \dot{\omega}_M + B_M \cdot \omega_M \quad (2.2)$$

$$k_T \cdot U_T = J_T \cdot \dot{\omega}_T + B_T \cdot \omega_T \quad (2.3)$$

k	proportionality constant
U	the input voltage
J	the moment of inertia
B	the linear friction
ω	the angular speed - the state variable of the helicopter
subscript M	related to or generated by main motor (or propeller)
subscript T	related to or generated by tail motor (or propeller)

The torque produced by motors is transformed to thrust via propellers.

2.2.3 Propellers

The torque generated by the main propeller is lifting up the helicopter while the tail propeller is ballancing the rotational torque produced by the main propeller and prevents the helicopter from spinning around.



Figure 2.4: Propeller - illustrative figure

The transfer characteristic of the angular speed of the motor and the torque generated by a propeller depends on the geometry of the propeller. In our case both propellers have got a fixed geometry with approximately quadratic characteristics. We will assume that each propeller has got the same characteristics in clockwise and anticlockwise directions.

$$M_{VM} = k_{2VM} \cdot \omega_M^2 + k_{1VM} \cdot \omega_M \quad (2.4)$$

$$M_{VT} = k_{2VT} \cdot \omega_T^2 + k_{1VT} \cdot \omega_T \quad (2.5)$$

$$M_{HM} = k_{2HM} \cdot \omega_M^2 + k_{1HM} \cdot \omega_M \quad (2.6)$$

$$M_{HT} = k_{2HT} \cdot \omega_T^2 + k_{1HT} \cdot \omega_T \quad (2.7)$$

M	torques generated by the propellers [N.m]
k_2, k_1	proportionality constants [kg.m.s^{-1}] and [kg.m]
subscript H	acting around the horizontal axis of rotation
subscript V	acting around the vertical axis of rotation

Each propeller influences both - azimuth and elevation angle of the helicopter. This property is called cross coupling between main and tail propellers and it is caused by the tilting of the spatulas (in our case constant). Putting this quality into formulas:

$$M_V = M_{VM} + M_{VT} \quad (2.8)$$

$$M_H = M_{HM} + M_{HT} - M_g \quad (2.9)$$

M_H, M_V	net torques produced by both propellers around both axes
M_g	moment caused by the gravity force acting on the helicopter

2.2.4 Mechanical parts

The dynamics of mechanical system of the helicopter is defined by the moment of inertia J and the friction B in both axes of rotation. Interesting fact to notice is that moment of inertia J depends on the center of gravity. Therefore it would have been correct to write $J(U_B)$, but we skip this notation assuming that the moment of inertia will be constant for a specific working point.

$$M_H = J_H \cdot \dot{\omega}_H + B_H \cdot \omega_H \quad (2.10)$$

$$M_V = J_V \cdot \dot{\omega}_V + B_V \cdot \omega_V \quad (2.11)$$

To make the system of the equations complete we will introduce two more equations defining the elevation and azimuth angles.

$$\dot{\psi} = \omega_H \quad (2.12)$$

$$\dot{\phi} = \omega_V \quad (2.13)$$

2.2.5 The subsystem interconnection

We rearrange obtained state equations such that all the derivatives of states are on the left hand sides of the equations. Rearranging (2.2) and (2.3) :

$$\dot{\omega}_M = -\frac{B_M}{J_M} \cdot \omega_M + \frac{k_M}{J_M} \cdot U_M \quad (2.14)$$

$$\dot{\omega}_T = -\frac{B_T}{J_T} \cdot \omega_T + \frac{k_T}{J_T} \cdot U_T \quad (2.15)$$

Substituting (2.4) and (2.5) into (2.8) (the same with (2.1),(2.6), (2.7) and (2.9))and rearranging:

$$\dot{\omega}_V = \frac{1}{J_V} (k_{2VM} \cdot \omega_M^2 + k_{1VM} \cdot \omega_M) + \frac{1}{J_V} (k_{2VT} \cdot \omega_T^2 + k_{1VT} \cdot \omega_T) - \frac{B_V}{J_V} \cdot \omega_V \quad (2.16)$$

$$\dot{\omega}_H = \frac{1}{J_H} (k_{2HM} \cdot \omega_M^2 + k_{1HM} \cdot \omega_M) + \frac{1}{J_H} (k_{2HT} \cdot \omega_T^2 + k_{1HT} \cdot \omega_T) - \frac{B_H}{J_H} \cdot \omega_H - \frac{k_B}{J_H} \cdot U_B \quad (2.17)$$

The state equations we have obtained are due to quadratic factors in (2.16) and (2.17) non-linear. One of the most common strategies how to obtain a state-space matrices of the non-linear system is to linearise it in a fixed working point.

2.2.6 The working point selection

We have already mentioned that the main requirement on the working point is that helicopter keeps its elevation angle and the azimuth angle constant while both motors are spinning around. If we assume that the center of gravity of the helicopter is fixed, i.e.:

$$U_{B0} = \text{const} \quad (2.18)$$

then the moments of inertia in the horizontal and vertical directions are also constant.

Therefore the equilibrium conditions are:

$$\omega_M = \omega_{M0} = \text{const}$$

$$\omega_T = \omega_{T0} = \text{const}$$

$$\omega_V = 0$$

$$\omega_H = 0$$

$$\psi = \psi_0 = \text{const}$$

$$\phi = \phi_0 = \text{const}$$

and all derivatives of states are equal to zero.

$$\dot{\omega}_M = \dot{\omega}_T = \dot{\omega}_V = \dot{\omega}_H = \dot{\psi} = \dot{\phi} = 0$$

To evaluate angular speeds of motors we substitute the equilibrium conditions into (2.16) and (2.17) obtaining:

$$\begin{aligned} 0 &= k_{2VM} \cdot \omega_{M0}^2 + k_{1VM} \cdot \omega_{M0} + k_{2VT} \cdot \omega_{T0}^2 + k_{1VT} \cdot \omega_{T0} \\ k_B \cdot U_{B0} &= k_{2HM} \cdot \omega_{M0}^2 + k_{1HM} \cdot \omega_{M0} + k_{2HT} \cdot \omega_{T0}^2 + k_{1HT} \cdot \omega_{T0} \end{aligned}$$

Assuming that for the higher rotation rates all $\omega_0^2 \gg \omega_0$ we can write:

$$\begin{aligned} k_{2VM} \cdot \omega_{M0}^2 &= -k_{2VT} \cdot \omega_{T0}^2 \\ k_B \cdot U_{B0} &= k_{2HM} \cdot \omega_{M0}^2 + k_{2HT} \cdot \omega_{T0}^2 \end{aligned}$$

After substituting and rearranging, we obtain linear dependence of the spinning rate of the main and tail propeller:

$$\begin{aligned} \omega_{M0} &= \sqrt{-\frac{k_{2VT}}{k_{2VM}}} \cdot \omega_{T0} \quad (2.19) \\ \omega_{M0} &= \sqrt{\frac{k_{2VT} \cdot k_B}{k_{2VT}k_{2HM} - k_{2HT}k_{2VM}}} \cdot \sqrt{U_{B0}} \\ \omega_{T0} &= \sqrt{\frac{k_{2VT} \cdot k_B}{k_{2VT}k_{2HM} - k_{2HT}k_{2VM}}} \cdot \sqrt{-\frac{k_{2VM}}{k_{2VT}}} \cdot \sqrt{U_{B0}} \end{aligned}$$

From the last two equations we can conclude that the relationship between the angular speeds of the main and tail motors (propellers) and the center of mass is quadratic.

The angular speeds of motors at equilibrium are defining equilibrium input voltages:

$$U_{M0} = \frac{B_M}{k_M} \cdot \omega_{M0} \quad U_{T0} = \frac{B_T}{k_T} \cdot \omega_{T0} \quad (2.20)$$

Evaluating equilibrium input voltages applied to tail motor in terms of main motor:

$$U_{T0} = \frac{\frac{B_T}{k_T}}{\frac{B_M}{k_M}} \cdot \sqrt{-\frac{k_{2VM}}{k_{2VT}}} \cdot U_{M0} \quad (2.21)$$

This equation proves the linear relationship between the input voltages applied to the system in various working points. The equations (2.21) and (2.19) will enable us to evaluate the transfer constants k_M and k_T of the motors if we knew the frictions in the motors B_M and B_T .

2.3 Linearization

2.3.1 The linearization of the state equations

We will obtain the linearized model by finding the first complete differential of non-linear model in the equilibrium position.

The complete differentials of the (2.14) and (2.15) are:

$$\begin{aligned} \dot{\omega}_{M0} - \partial\dot{\omega}_M &= -\frac{B_M}{J_M} \cdot (\omega_{M0} - \partial\omega_M) + \frac{k_M}{J_M} \cdot (U_{M0} - \partial U_M) \\ \dot{\omega}_{T0} - \partial\dot{\omega}_T &= -\frac{B_T}{J_T} \cdot (\omega_{T0} - \partial\omega_T) + \frac{k_T}{J_T} \cdot (U_{T0} - \partial U_T) \end{aligned}$$

The complete differentials of the (2.16) and (2.17) are:

$$\begin{aligned} 0 - \partial\dot{\omega}_V &= \frac{1}{J_V} (2k_{2VM} \cdot \omega_{M0} + k_{1VM}) (\omega_{M0} - \partial\omega_M) + \\ &\quad + \frac{1}{J_V} (2k_{2VT} \cdot \omega_{T0} + k_{1VT}) (\omega_{T0} - \partial\omega_T) - \\ &\quad - \frac{B_V}{J_V} (0 - \partial\omega_V) \\ 0 - \partial\dot{\omega}_H &= \frac{1}{J_H} (2k_{2HM} \cdot \omega_{M0} + k_{1HM}) (\omega_{M0} - \partial\omega_M) + \\ &\quad + \frac{1}{J_H} (2k_{2HT} \cdot \omega_{T0} + k_{1HT}) (\omega_{T0} - \partial\omega_T) - \\ &\quad - \frac{B_H}{J_H} (0 - \partial\omega_H) - \frac{k_B}{J_H} (U_{B0} - \partial U_B) \end{aligned}$$

Finally the complete differentials of the (2.12) and (2.13) are:

$$\begin{aligned}\dot{\psi}_0 - \partial\psi &= 0 - \partial\omega_H \\ \dot{\phi}_0 - \partial\phi &= 0 - \partial\omega_V\end{aligned}$$

Now we subtract out the equilibrium solution (assuming the deviation $\partial U_B = 0$). From now on we skip the ∂ notation assuming all state variables are referring to deviations from the equilibrium, thus:

$$\dot{\omega}_M = -\frac{B_M}{J_M} \cdot \omega_M + \frac{k_M}{J_M} \cdot U_M \quad (2.22)$$

$$\dot{\omega}_T = -\frac{B_T}{J_T} \cdot \omega_T + \frac{k_T}{J_T} \cdot U_T \quad (2.23)$$

$$\begin{aligned}\dot{\omega}_V = \frac{1}{J_V} (2k_{2VM} \cdot \omega_{M0} + k_{1VM})\omega_M + \frac{1}{J_V} (2k_{2VT} \cdot \omega_{T0} + k_{1VT})\omega_T - \\ -\frac{B_V}{J_V} \cdot \omega_V\end{aligned} \quad (2.24)$$

$$\begin{aligned}\dot{\omega}_H = \frac{1}{J_H} (2k_{2HM} \cdot \omega_{M0} + k_{1HM})\omega_M + \frac{1}{J_H} (2k_{2HT} \cdot \omega_{T0} + k_{1HT})\omega_T - \\ -\frac{B_H}{J_H} \cdot \omega_H\end{aligned} \quad (2.25)$$

$$\dot{\psi} = \omega_H \quad (2.26)$$

$$\dot{\phi} = \omega_V \quad (2.27)$$

Now we are ready to construct a continuous in time state-space model of the system.

2.4 State space model

2.4.1 State space matrices

We construct of the state space description of the system from the (2.22), (2.23), (2.24) and (2.25). To keep the transparency of the system analysis we introduce few substitutions:

$$p_M = \frac{B_M}{J_M} \quad p_T = \frac{B_T}{J_T} \quad p_V = \frac{B_V}{J_V} \quad p_H = \frac{B_H}{J_H} \quad (2.28)$$

$$\rho_{VM} = \frac{1}{J_V} (2k_{2VM} \cdot \omega_{M0} + k_{1VM})$$

$$\rho_{VT} = \frac{1}{J_V} (2k_{2VT} \cdot \omega_{T0} + k_{1VT})$$

$$\rho_{HM} = \frac{1}{J_H} (2k_{2HM} \cdot \omega_{M0} + k_{1HM})$$

$$\rho_{HT} = \frac{1}{J_H} (2k_{2HT} \cdot \omega_{T0} + k_{1HT})$$

We define input, output and state vector:

$$\mathbf{u} = \begin{pmatrix} U_M & U_T \end{pmatrix}^T \quad (2.29)$$

$$\mathbf{y} = \begin{pmatrix} \psi & \phi \end{pmatrix}^T \quad (2.30)$$

$$\mathbf{x} = \begin{pmatrix} \omega_M & \omega_T & \omega_V & \omega_H & \psi & \phi \end{pmatrix}^T \quad (2.31)$$

The matrix form we obtain is:

$$\dot{\mathbf{x}} = \mathbf{A}\mathbf{x} + \mathbf{B}\mathbf{u}$$

$$\mathbf{y} = \mathbf{C}\mathbf{x} + \mathbf{D}\mathbf{u}$$

Where matrices \mathbf{A} , \mathbf{B} , \mathbf{C} and \mathbf{D} are representing state space model of the system:

$$\mathbf{A} = \begin{pmatrix} -p_M & 0 & 0 & 0 & 0 & 0 \\ 0 & -p_T & 0 & 0 & 0 & 0 \\ \rho_{VM} & \rho_{VT} & -p_V & 0 & 0 & 0 \\ \rho_{HM} & \rho_{HT} & 0 & -p_H & 0 & 0 \\ 0 & 0 & 0 & 1 & 0 & 0 \\ 0 & 0 & 1 & 0 & 0 & 0 \end{pmatrix} \quad \mathbf{B} = \begin{pmatrix} \frac{k_M}{J_M} & 0 \\ 0 & \frac{k_T}{J_T} \\ 0 & 0 \\ 0 & 0 \\ 0 & 0 \\ 0 & 0 \end{pmatrix} \quad (2.32)$$

$$\mathbf{C} = \begin{pmatrix} 0 & 0 & 0 & 0 & 1 & 0 \\ 0 & 0 & 0 & 0 & 0 & 1 \end{pmatrix} \quad \mathbf{D} = \begin{pmatrix} 0 & 0 \\ 0 & 0 \end{pmatrix}$$

Performing the Laplace transformation

$$\begin{aligned} s\mathbf{X}(s) - \mathbf{x}(0) &= \mathbf{A} \cdot \mathbf{X}(s) + \mathbf{B} \cdot \mathbf{U}(s) \\ \mathbf{Y}(s) &= \mathbf{C} \cdot \mathbf{X}(s) + \mathbf{D} \cdot \mathbf{U}(s) \end{aligned} \quad (2.33)$$

Where

$$\mathbf{x}(0) = \left(\omega_{M0} \quad \omega_{T0} \quad 0 \quad 0 \quad \psi_0 \quad \phi_0 \right)^T \quad (2.34)$$

- X Laplace transformation of a state vector of the system
- $x(0)$ state vector defining equilibrium of the system
- U Laplace transformation of an input vector of the system
- Y Laplace transformation of an output vector of the system

The Fig. 2.5 illustrates the role of each matrix. We see that the matrix \mathbf{A} is a feedback matrix also called a **system matrix**, matrix \mathbf{B} is an input matrix, matrix \mathbf{C} is an output matrix and matrix \mathbf{D} is a direct transmission matrix.

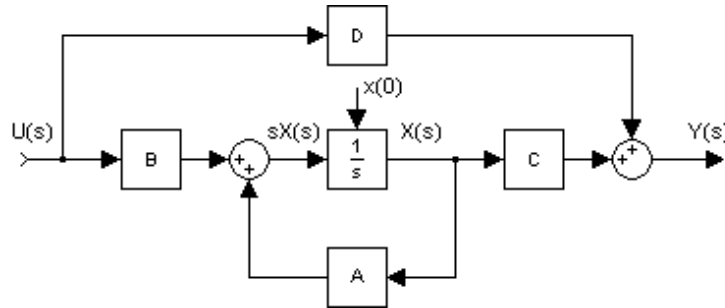


Figure 2.5: The state space model

2.4.2 From the state space description to the transfer matrix

We will base out transfer matrix derivation on the fact of zero initial conditions:

$$\mathbf{x}(0) = 0 \quad (2.35)$$

Thus the equation (2.33) will change into:

$$s\mathbf{X}(s) = \mathbf{A} \cdot \mathbf{X}(s) + \mathbf{B} \cdot \mathbf{U}(s) \quad (2.36)$$

$$\mathbf{Y}(s) = \mathbf{C} \cdot \mathbf{X}(s) + \mathbf{D} \cdot \mathbf{U}(s) \quad (2.37)$$

Evaluating $\mathbf{X}(s)$ from the (2.36) :

$$\mathbf{X}(s) = (s\mathbf{I} - \mathbf{A})^{-1} \mathbf{B} \cdot \mathbf{U}(s)$$

We obtain the transfer matrix by substituting obtained $\mathbf{X}(s)$ into output equation (2.37) and rearranging:

$$\mathbf{G}(s) = \frac{\mathbf{Y}(s)}{\mathbf{U}(s)} = \mathbf{C}(s\mathbf{I} - \mathbf{A})^{-1} \mathbf{B} + \mathbf{D}$$

To balance the assumption (2.35) we will need to set the system into the equilibrium position externally Fig. 2.6.

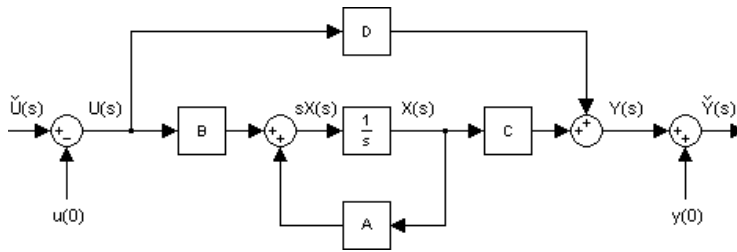


Figure 2.6: The modified state space model for the zero initial conditions

Where the input and output vectors are

$$\check{\mathbf{U}}(s) = \mathbf{U}(s) + \mathbf{u}(0) \quad \check{\mathbf{Y}}(s) = \mathbf{Y}(s) + \mathbf{y}(0) \quad (2.38)$$

and

$$\mathbf{u}(0) = (U_{M0} \quad U_{T0})^T \quad \mathbf{y}(0) = (\psi_0 \quad \phi_0)^T \quad (2.39)$$

$u(0)$ the necessary constant input vector to keep the system in equilibrium

$y(0)$ the constant output vector when the system is in equilibrium

Before we evaluate the transfer matrix let us introduce following substitutions:

$$\kappa_{HM} = \rho_{HM} \frac{k_M}{J_M} \quad \kappa_{HT} = \rho_{HT} \frac{k_T}{J_T} \quad \kappa_{VM} = \rho_{VM} \frac{k_M}{J_M} \quad \kappa_{VT} = \rho_{VT} \frac{k_T}{J_T} \quad (2.40)$$

The transfer matrix of the helicopter model is:

$$\mathbf{G}(s) = \begin{pmatrix} G_{HM} & G_{HT} \\ G_{VM} & G_{VT} \end{pmatrix} = \begin{pmatrix} \frac{\kappa_{HM}}{s(s+p_H)(s+p_M)} & \frac{\kappa_{HT}}{s(s+p_H)(s+p_T)} \\ \frac{\kappa_{VM}}{s(s+p_V)(s+p_M)} & \frac{\kappa_{VT}}{s(s+p_V)(s+p_T)} \end{pmatrix} \quad (2.41)$$

We see that each of the partial transfer functions G_{HM}, G_{HT}, G_{VM} and G_{VT} are of the third order and have the same form:

$$G(s) = \frac{\kappa}{s(s+a)(s+b)} \quad (2.42)$$

Assuming the system (2.42) is asymptotically stable we expect it to perform following responses:

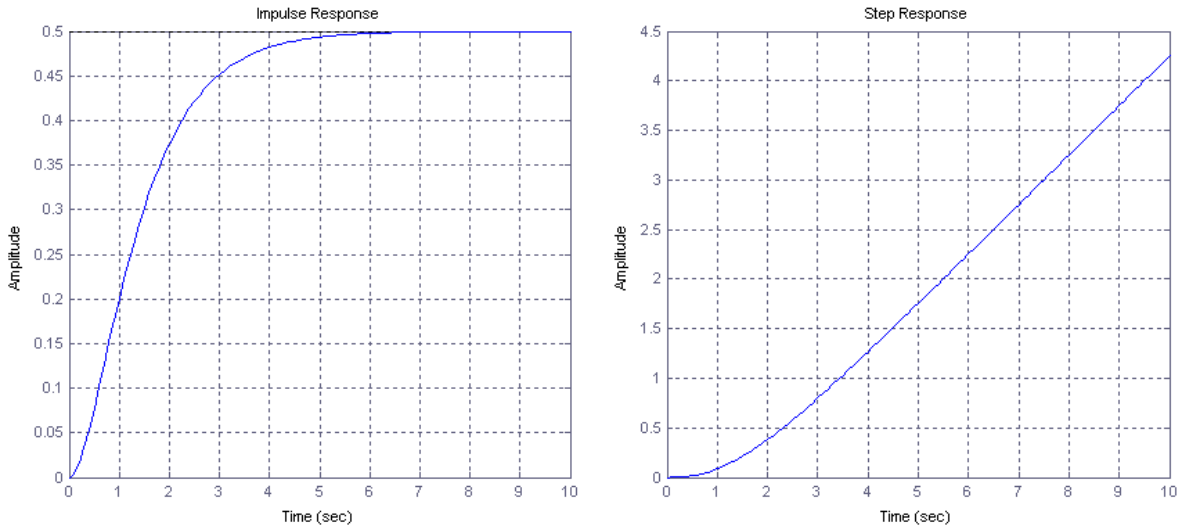


Figure 2.7: The impulse and step response of the system $G(s)$

Due to the friction B_H and B_V the helicopter will get to rest if disturbed by short pulse. If the constant torque is applied to the horizontal or vertical axis of rotation the helicopter will turn around with constant angular speed.

The following chapter will examine the step responses of $G(s)$ closer.

Chapter 3

Identification methods

This chapter will introduce strategies and methods necessary for the system identification. We start with investigation of the static characteristics where we discuss a method for equilibrium estimation and a method for estimation of the steady spinning rate of the motors.

We continue with dynamic characteristics investigation. Close look to the step responses of the system enables us to find transfer matrix $\mathbf{G}(s)$ of the system. At the end of this chapter we will combine the data obtained from static and dynamic characteristics to evaluate all the necessary parameters for the continuous state space model of the system.

3.1 Static characteristics

3.1.1 Strategies for static experiments

We start the system identification with finding out all the operation ranges of input voltages and output angles. Hence we find the scaling constants between the output units and radians to scale the outputs.

Measuring characteristics of the system in equilibrium positions for various positions of the center of gravity will enable us to select the working points in which we will investigate the dynamic responses of the system.

We will also need to measure the steady state spinning rate of motors and propellers. This experiment, together with results from the dynamic responses will enable us to estimate parameters of the continuous state space model of the system.

3.1.2 Equilibria

For the fixed position of the center of gravity of the helicopter defined by (2.18) we find the equilibrium input vector (2.39). We repeat this measurement for the whole range of the center of gravity positions - U_B .

The measured relationship between the input voltage applied on the main motor and the input voltage applied on the tail motor we expect to be linear according to (2.21). We select the working points such that they are as far as possible from each other but still lying in the linear region.

3.1.3 Steady state spinning rate of motors

The experiment for the steady state spinning rate of motors will require a special apparatus because the angular frequencies of the motors are not measured and provided for user. This experiment is crucial for the evaluation of the proportionality constants of motors k_M and k_T (see (2.2) and (2.3)).

We will measure the dependence of the angular frequency of motor with propeller on the applied voltage. To see the expected relationship clearly we need to rearrange the (2.20) into following form:

$$\omega_{M0} = \frac{k_M}{B_M} \cdot U_{M0} \quad \omega_{T0} = \frac{k_T}{B_T} \cdot U_{T0} \quad (3.1)$$

From (3.1) we see that the expected relationship is linear with slopes defining the $\frac{k_M}{B_M}$ and $\frac{k_T}{B_T}$ ratios.

The parameters we are looking for are $\frac{B_M}{k_M}$ and $\frac{B_T}{k_T}$ therefore we will have to take **inverted** values of the estimated slopes:

$$\frac{B_M}{k_M} = \frac{\partial U_{M0}}{\partial \omega_{M0}} \quad \frac{B_T}{k_T} = \frac{\partial U_{T0}}{\partial \omega_{T0}} \quad (3.2)$$

which are in fact slopes of the former functions (2.2) and (2.3).

3.2 Dynamic characteristics

3.2.1 Strategies for the evaluation of dynamic responses

To identify the system we have chosen to start with the simplest and the most evident responses and then proceed to more complicated ones. The simplicity has to be conserved through whole identification to make it transparent and easy to follow.

Linearised model is approximating the behavior of the non-linear model near to the working point, therefore we begin with identifying the range of amplitudes of input signal that are exciting the system enough but not too much.

When all this is done we are ready to analyze the step responses of the system Fig. 3.1.

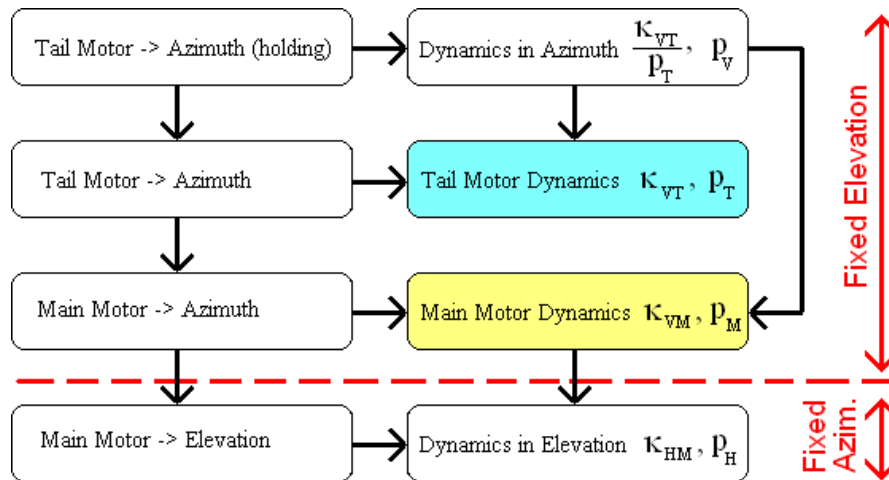


Figure 3.1: Motors dynamics identification strategy

We continue with identification of the systems dynamics around the vertical axis of rotation therefore we fix the helicopter in elevation.

To separate the transient response of the tail motor and mechanical part of the system we hold the helicopter until the spinning rate of the tail motor is constant (clearly hearable). At this moment the torque applied around the vertical axis of rotation is constant and after releasing the helicopter we read pure transient response of the mechanics.

We do the same experiment without holding the model to identify the overall dynamics around the vertical axis of rotation. The tail motors dynamics can be extracted from previous two experiments.

The identification of the dynamics of both motors is therefore done indirectly through the dynamics mechanical parts of the system.

Knowing the transient response of the mechanics around the vertical axis of rotation and measuring the step responses of main motor we can find main motor dynamics.

Now we are ready to identify the systems behaviour around the horizontal axis of rotation therefore we fix the helicopter in azimuth.

We measure the step responses of the system around the horizontal axis of rotation. Knowing the main motor dynamics we can extract the dynamics of mechanics from this measurement.

The influence of the tail motor around the horizontal axis of rotation is very small and not measurable in linear region. Therefore we will neglect it during the identification considering the proportional factor to be small constant (nearly zero).

To the rest of the working points we take the information of motors' dynamics and identify only the dynamics of the mechanical parts of the system (which are mass point dependent).

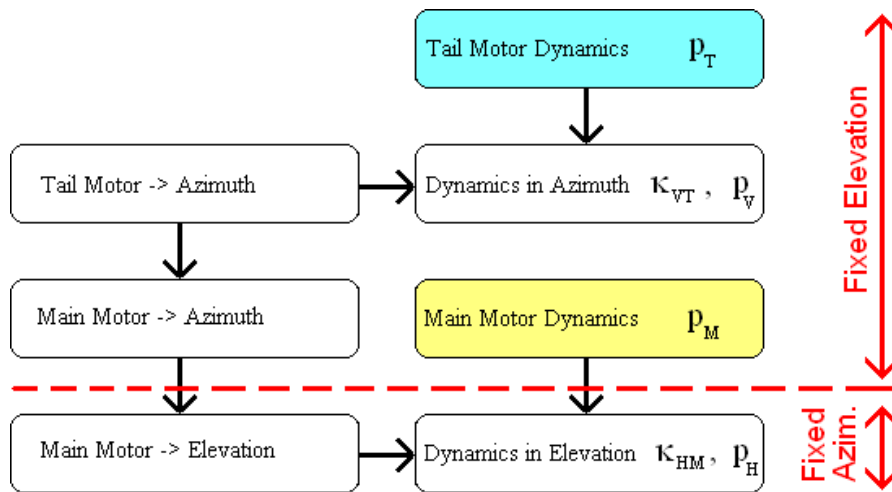


Figure 3.2: Identification strategy for the rest of working points

It is important to notice that the error, in this strategy, is cumulative therefore the better the identification of the motors at the beginning the better the overall system identification.

3.2.2 The first algorithm for step response evaluation

We will investigate the separation of the dynamics of motor and mechanics closer in general form. The biggest advantage of the algorithm we are going to describe now is

that it does not need any a priori information about the system. Therefore it is good to start the system identification with this algorithm to obtain some useful parameters and ratios for the further investigation.

Let us consider a stable system with the transfer function in the form (2.42):

$$G(s) = \frac{\kappa}{s(s+a)(s+b)} = \frac{\frac{\kappa}{b}}{a-b} \left(\frac{1}{s+a} - \frac{1}{s+b} \right) + \frac{\frac{\kappa}{b}}{s(s+a)} = H(s) + F(s)$$

$a, b, c, d \in \mathbf{R}_+$... are constants

$$\text{where } H(s) = \frac{\frac{\kappa}{b}}{a-b} \left(\frac{1}{s+a} - \frac{1}{s+b} \right) \quad \text{and} \quad F(s) = \frac{\frac{\kappa}{b}}{s(s+a)}$$

The step response of the $G(s)$ is:

$$g(t) = \tilde{g}(t) + \hat{g}(t) = \frac{\kappa}{(a-b)(ab)^2} \left(a^2 \cdot \exp(-b.t) - b^2 \cdot \exp(-a.t) \right) + \frac{\kappa}{ab} t - \frac{\kappa(a+b)}{(ab)^2} \quad (3.3)$$

where homogenous solution and particular solution are represented by:

$$\tilde{g}(t) = \frac{\kappa}{(a-b)(ab)^2} \left(a^2 \cdot \exp(-b.t) - b^2 \cdot \exp(-a.t) \right) \quad \text{and} \quad \hat{g}(t) = \frac{\kappa}{ab} t - \frac{\kappa(a+b)}{(ab)^2}$$

The step response of the $F(s)$ is:

$$f(t) = \tilde{f}(t) + \hat{f}(t) = \frac{\kappa}{a^2b} \exp(-at) + \frac{\kappa}{ab} t - \frac{\kappa}{a^2b}$$

where homogenous solution and particular solution are represented by:

$$\tilde{f}(t) = \frac{\kappa}{a^2b} \exp(-at) \quad \text{and} \quad \hat{f}(t) = \frac{\kappa}{ab} t - \frac{\kappa}{a^2b}$$

The particular solutions $\hat{g}(t)$ and $\hat{f}(t)$ can be formally rewritten into the form:

$$\hat{f}(t) = \frac{\kappa}{ab}t - \frac{\kappa}{a^2b} = m\left(t - \frac{1}{a}\right) = m \cdot t + \hat{f}(0) \quad (3.4)$$

$$\hat{g}(t) = \frac{\kappa}{ab}t - \frac{\kappa(a+b)}{(ab)^2} = m\left(t - \left(\frac{1}{a} + \frac{1}{b}\right)\right) = m \cdot t + \hat{g}(0) \quad (3.5)$$

where

$$m = \frac{\kappa}{ab} \quad \therefore \quad \kappa = abm \quad (3.6)$$

$$\hat{f}(0) = -\frac{m}{a} \quad \therefore \quad a = -\frac{m}{\hat{f}(0)} \quad (3.7)$$

$$\hat{g}(0) = -m\left(\frac{1}{a} + \frac{1}{b}\right) \quad \therefore \quad b = \frac{m \cdot a}{a \cdot \hat{g}(0) - m} = \frac{m}{\hat{f}(0) - \hat{g}(0)} \quad (3.8)$$

From the equations (3.4) and (3.5) it is evident that the $\hat{f}(t)$ and $\hat{g}(t)$ must be parallel as it is shown on the Fig. 3.3 because both of them have the same slope m .

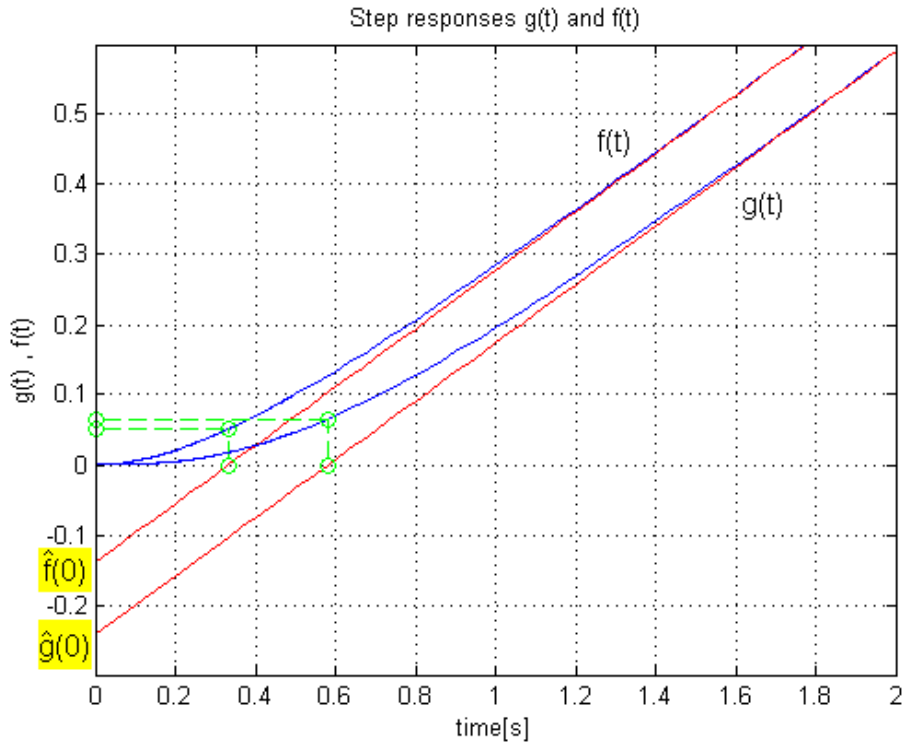


Figure 3.3: The dynamics separation identification algorithm

3.2.3 The limits of the first algorithm

The first algorithm that we have described is based on the assumption that the experiment will last long enough for transient responses to fade out. If this condition is not full filled we obtain wrong results. The Fig. 3.4 shows that the particular solutions $\hat{g}(t)$ and $\hat{f}(t)$ are not parallel any more if the experiment time is short.

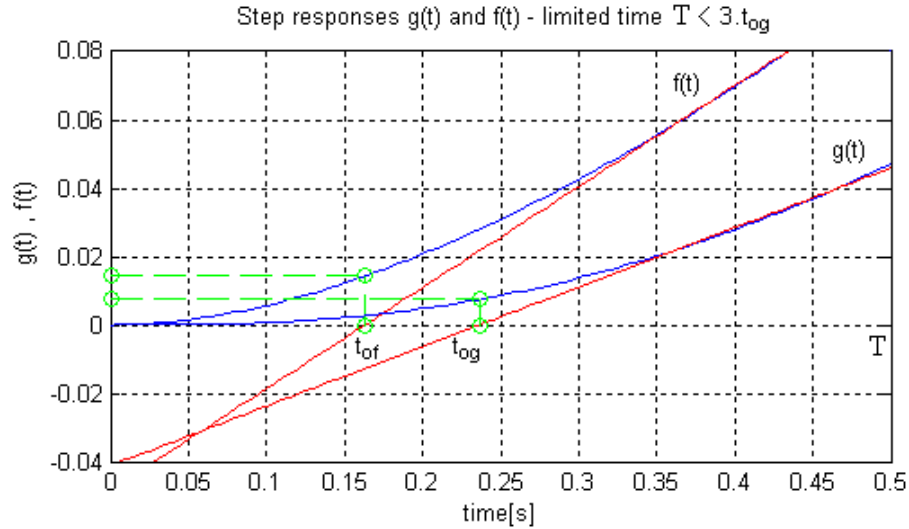


Figure 3.4: Short time step response experiment - wrong results

If we denote the time of experiment T and

$$\hat{f}(t_{of}) = 0 \qquad \hat{g}(t_{og}) = 0$$

then the first algorithm is trustworthy if

$$T > 3 \cdot t_{of} \qquad T > 3 \cdot t_{og}$$

T the time of the experiment

If this condition is not full filled we have to rely on the information we have already obtained from previous measurements and try the second algorithm for the step response evaluation.

3.2.4 The second algorithm for step response evaluation

The development of the second algorithm for step response evaluation is motivated by the fact that the helicopter has edge stoppers at both ends of each axis of rotation which are preventing it from spinning around. Thus the longest time for the experiment is defined by the time needed for the helicopter to move from one end to another.

Knowing that $f(t)$ response is faster than $g(t)$ we can estimate constants m and a from the first algorithm and use them to find b and κ in the algorithm we are going to describe now.

The time requirements of the second algorithm are following:

$$T > t_{og} \quad T_s \rightarrow 0$$

T the time of the experiment

T_s the sampling time

From the (3.3) using the substitution (3.6) we derive:

$$g(m, a, b, t) = \frac{m}{ab(a-b)} \left(a^2 \cdot \exp(-b.t) - b^2 \cdot \exp(-a.t) \right) + mt - \frac{m(a+b)}{ab}$$

If we know parameters m and a we can estimate the parameter using the measured $g_M(t)$ and the function:

$$g(m, a, \frac{1}{t}, t) = \frac{mt}{a(a - \frac{1}{t})} \left(a^2 \cdot \exp(-1) - \frac{1}{t^2} \cdot \exp(-a.t) \right) + mt - \frac{mt(a + \frac{1}{t})}{a} \quad (3.9)$$

Let us define artificial $z(t)$ function:

$$z(t) = |g_M(t) - g(m, a, \frac{1}{t}, t)|$$

Then the parameter b is found from:

$$b = \frac{1}{\min(z(t))} \quad (3.10)$$

and parameter κ from the equation (3.6)

The Fig. 3.5 shows the use of the $z(t)$ function.

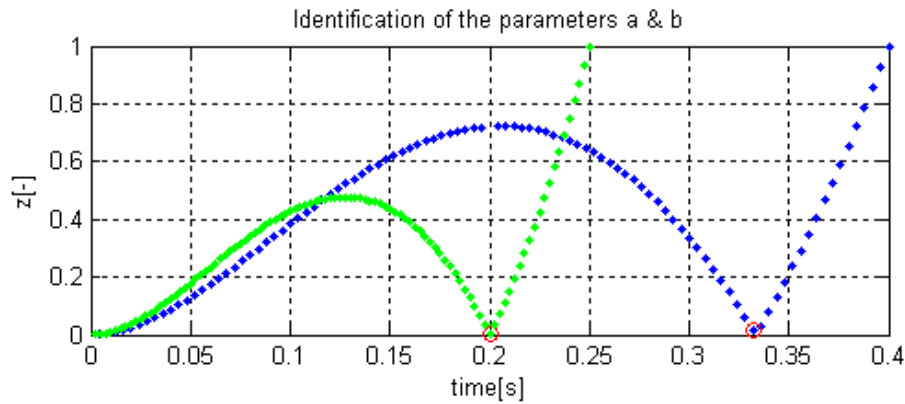


Figure 3.5: $z(t)$ function

3.2.5 The limits of the second algorithm

The second algorithm that we have described is based on the equation (3.9) and the domain of $g(m, a, \frac{1}{t}, t)$ function is defined as:

$$\begin{aligned} t &> 0 \\ a &\neq 0 \\ b &\neq 0 \\ a &\neq \frac{1}{t} \end{aligned}$$

It is also important to notice that the z function has got always two local minimas Fig. 3.5. The first one is near to the origin and the second one characterises the missing parameter.

We will have to keep in mind these constraints while implementing the z function algorithm.

3.2.6 The state space model evaluation

The evaluation of the dynamic responses of the system will enable us to identify the transfer matrix of the system (2.41) with parameters:

$$p_M, \quad p_T, \quad p_V, \quad p_H, \quad \kappa_{HM}, \quad \kappa_{HT}, \quad \kappa_{VM}, \quad \kappa_{VT}$$

Before we start with evaluation of the missing constants let us recall equations (3.2):

$$\frac{B_M}{k_M} = \frac{\partial U_{M0}}{\partial \omega_{M0}} \quad \frac{B_T}{k_T} = \frac{\partial U_{T0}}{\partial \omega_{T0}}$$

and the substitutions we made (2.28):

$$p_M = \frac{B_M}{J_M} \quad p_T = \frac{B_T}{J_T}$$

From these equations we can extract the constants of motors:

$$\frac{k_M}{J_M} = \frac{p_M}{\frac{B_M}{k_M}} \quad \text{and} \quad \frac{k_T}{J_T} = \frac{p_T}{\frac{B_T}{k_T}} \quad (3.11)$$

The ρ parameters of the state space model are evaluated from the substitution into rearranged (2.40)

$$\rho_{VM} = \frac{\kappa_{VM}}{\frac{k_M}{J_M}} \quad \rho_{HM} = \frac{\kappa_{HM}}{\frac{k_M}{J_M}} \quad \rho_{VT} = \frac{\kappa_{VT}}{\frac{k_T}{J_T}} \quad \rho_{HT} = \frac{\kappa_{HT}}{\frac{k_T}{J_T}} \quad (3.12)$$

Chapter 4

System Identification

4.1 Static characteristics

4.1.1 Ranges and the conversion of units

Our initial experiment is to identify the limits of the azimuth and the elevation angles and the limits of the input voltages applied.

After identifying the operation ranges we proceed with identifying the conversion constants because we would like to obtain the azimuth and elevation angles in radians and input voltages in volts (not in the MATLAB units [MU] and [MP]).

Table 4.1: The input and output vector ranges and conversion constants

quantity	from [MU]	to [MU]	conversion constant [V]/[MU]
U_M	-1	1	12/1
U_T	-1	1	6/1
U_B	-0.9	-0.8	1
quantity	from [MP]	to [MP]	conversion constant [rad]/[MP]
ϕ	0	365	$\frac{\pi}{256}$
ψ	0	135	$\frac{\pi}{256}$

We decided to convert all physical quantities into the Matlab units to make the identification results compatible with the control synthesis.

4.1.2 Static equilibria characteristics

We proceed with measurement of static equilibria. Each equilibrium is measured for the constant time interval $t = 60\text{sec}$ and the main criterion is that the helicopter moves not more than $\pm 10\circ$.

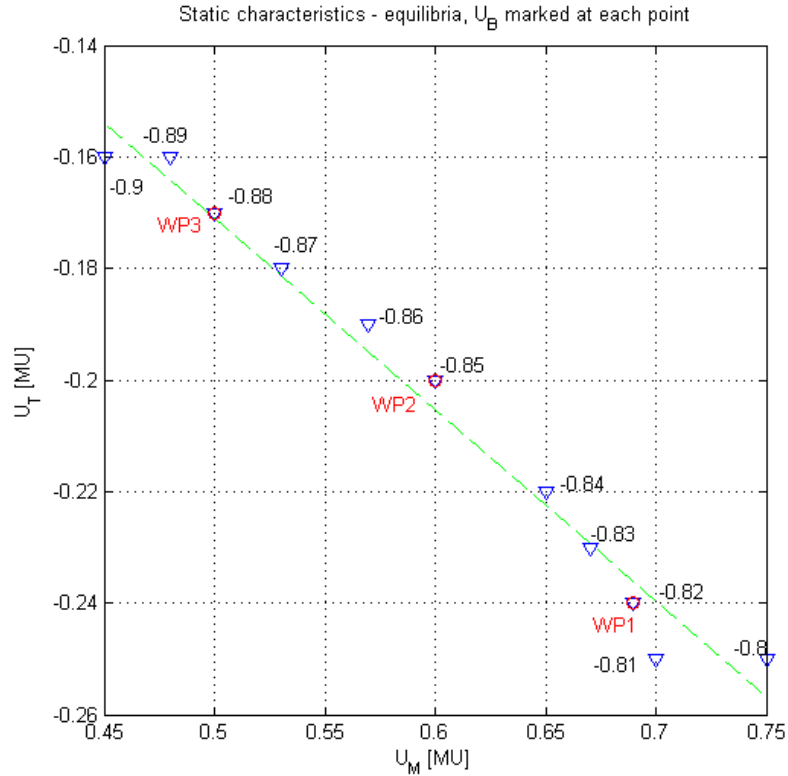


Figure 4.1: Static characteristics - equilibria measurement

Using the linear interpolation we approximate the slope from equation (2.21) of the equilibrium characteristics Fig. 4.1:

$$\frac{\partial U_{T0}}{\partial U_{M0}} = \frac{\frac{B_T}{k_T}}{\frac{B_M}{k_M}} \cdot \sqrt{-\frac{k_{2VM}}{k_{2VT}}} = -0.343[-] \quad (4.1)$$

We have selected three working points which lie in the linear region, marked with red circles Fig. 4.1.

4.1.3 Steady state spinning rate of motors

To measure the steady state spinning rate of motors we need an apparatus that will count the turns of the propeller without affecting its dynamics. We decided to build a simple schematics that will be based on slotted opto sensor. The circuit is shown of the Fig. 4.2

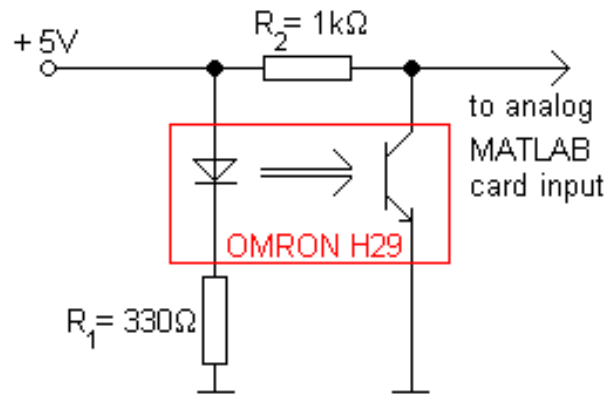


Figure 4.2: Schematics for the slotted optosensor interconnection

We have fixed the sensor to ensure standard conditions for all measurements Fig. 4.3.



Figure 4.3: The settings of the experiment

It is worth noticing that the sampling time for this experiment has to be very short. Thus we have set the sampling time to $T_s = 0.1ms$.

The data taken from the analog input was noisy but complete. We got rid out of the noise during the singal post processing.

The resultant characteristics of the spinning rate of the main motor is on the Fig. 4.4

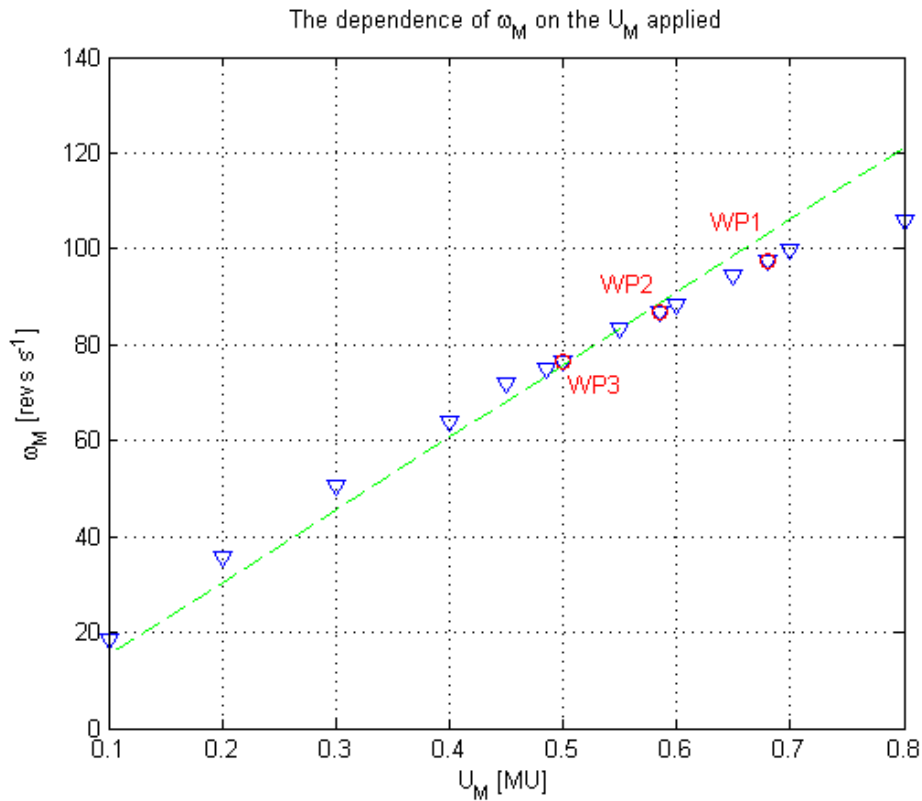


Figure 4.4: The steady state spinning rate of the main motor

Form the slope of this characteristics we can evaluate the $\frac{k_M}{B_M}$ constant using (2.14):

$$\frac{k_M}{B_M} = \frac{\partial \omega_{M0}}{\partial U_{M0}} = 79.3[\text{rad.s}^{-1}.\text{V}^{-1}] = 152[\text{revs}/\text{MU}]$$

then the substitution into (3.2) will give us:

$$\frac{B_M}{k_M} = 0.0126[\text{V.s.rad}^{-1}] = 0.0066[\text{MU}/\text{revs}]$$

The unit **revs** stands for **revolutions**.

The resultant characteristics of the spinning rate of the tail motor is on the Fig. 4.5

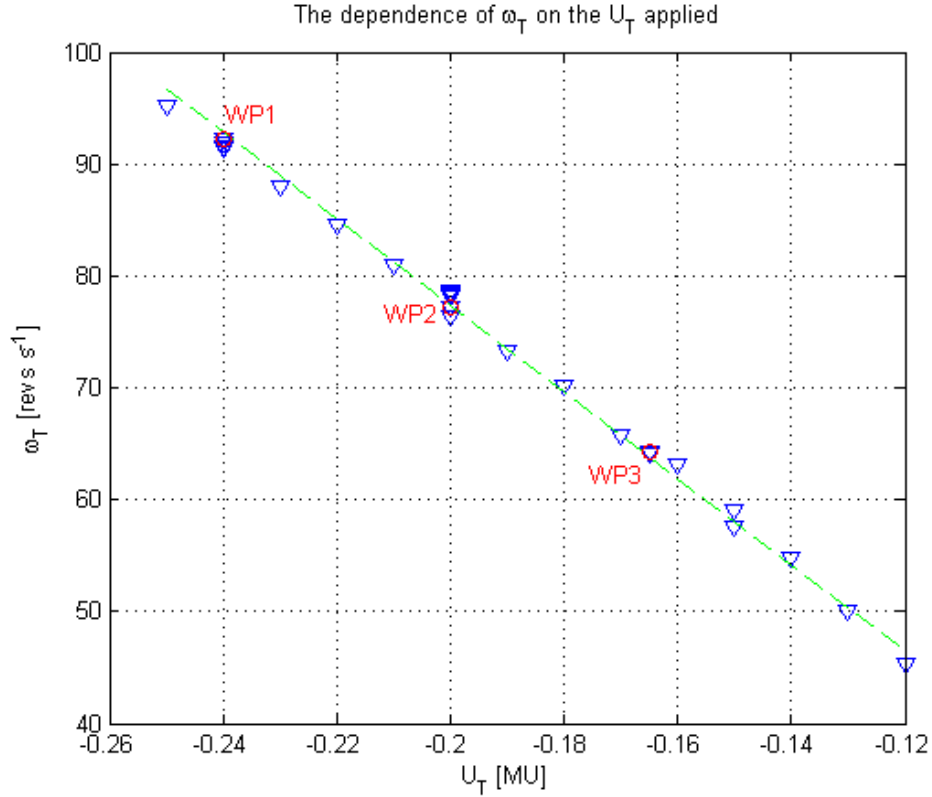


Figure 4.5: The steady state spinning rate of the tail motor

Form the slope of this characteristics we can evaluate the $\frac{k_T}{B_T}$ constant using (2.15):

$$\frac{k_T}{B_T} = \frac{\partial \omega_{T0}}{\partial U_{T0}} = -405[\text{rad.s}^{-1}.\text{V}^{-1}] = -387[\text{revs/MU}]$$

then the substitution into (3.2) will give us:

$$\frac{B_T}{k_T} = -0.0025[\text{V.s.rad}^{-1}] = -0.0026[\text{MU/revs}]$$

The minus sign in the result indicates the opposite spinning direction to the main motor.

The interesting result is from the mutual spinning rate characteristics Fig. 4.6

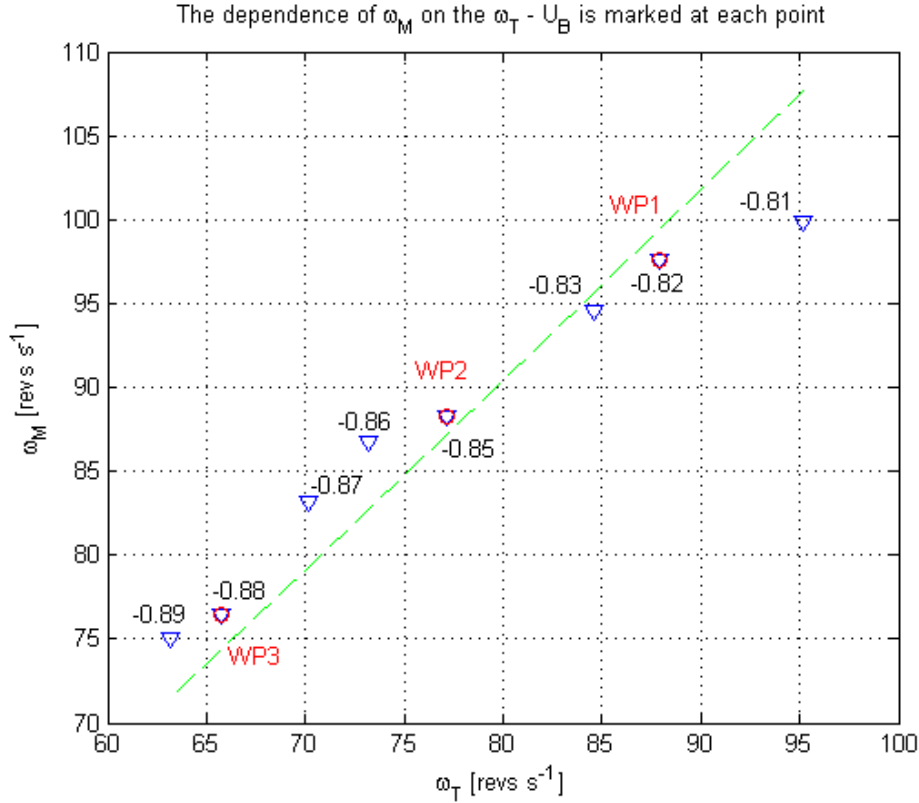


Figure 4.6: The mutual steady state spinning rate characteristics

Form the slope of this characteristics we can evaluate the $\sqrt{-\frac{k_{2VT}}{k_{2VM}}}$ constant using (2.19):

$$\sqrt{-\frac{k_{2VT}}{k_{2VM}}} = \frac{\partial \omega_{M0}}{\partial \omega_{T0}} = 1.13[-]$$

The inverse value is then:

$$\sqrt{-\frac{k_{2VM}}{k_{2VT}}} = 0.885[-]$$

Now we are ready to prove the accuracy of our measurement by substituting into (4.1)

$$\frac{\partial U_{T0}}{\partial U_{M0}} = \frac{\frac{B_T}{k_T}}{\frac{B_M}{k_M}} \cdot \sqrt{-\frac{k_{2VM}}{k_{2VT}}} = \frac{152}{-387} \cdot 0.885 = -0.345[-]$$

We compare the obtained result with the result measured in (4.1) concluding that the static characteristics measurements have been done accurately.

4.1.4 Initial conditions

Before we move to identification of the dynamics of the model we briefly sum up the initial conditions that we have obtained from the static characteristics. The tables 4.2, 4.3 and 4.4 show all non-zero components of initial input and state vectors.

Table 4.2: Input $u(0)$ and state $x(0)$ vectors for the working point 1

quantity	in Matlab units	in SI units
U_{M0}	0.68	8.16 [V]
U_{T0}	-0.24	-1.44 [V]
U_{B0}	-0.82	-0.82 [V]
ω_{M0}	98 [revs. s^{-1}]	613 [rad. s^{-1}]
ω_{T0}	92 [revs. s^{-1}]	577 [rad. s^{-1}]

Table 4.3: Input $u(0)$ and state $x(0)$ vectors for the working point 2

quantity	in Matlab units	in SI units
U_{M0}	0.585	7.02 [V]
U_{T0}	-0.20	-1.20 [V]
U_{B0}	-0.85	-0.85 [V]
ω_{M0}	87 [revs. s^{-1}]	545 [rad. s^{-1}]
ω_{T0}	78 [revs. s^{-1}]	490 [rad. s^{-1}]

Table 4.4: Input $u(0)$ and state $x(0)$ vectors for the working point 3

quantity	in Matlab units	in SI units
U_{M0}	0.485	5.82 [V]
U_{T0}	-0.165	-0.99 [V]
U_{B0}	-0.88	-0.88 [V]
ω_{M0}	75 [revs. s^{-1}]	471 [rad. s^{-1}]
ω_{T0}	64 [revs. s^{-1}]	403 [rad. s^{-1}]

The initial output vector $y(0)$ in all three cases is a zero vector.

4.2 Dynamic characteristics

We decided to start the identification of the system from the second working point because it is placed in the middle of the linear region. The following section shows the procedure of the identification of the second working point and at the end sums up all the results obtained from identification of all three working points.

4.2.1 The input signal

The transient responses with initial 'holding' of the helicopter are measured all with constant input vector. The amplitude of the input vector are calculated from (4.2) such that the step jumps are proportional to the torques generated around vertical or horizontal axis of rotation:

$$\begin{pmatrix} \alpha_{MAX} \\ \alpha_{MIN} \end{pmatrix} = \begin{pmatrix} \sqrt{1 + perc/100} - 1 \\ \sqrt{1 - perc/100} - 1 \end{pmatrix} U_0 \quad (4.2)$$

- α amplitude of the step jumps (maximal and minimal)
- $perc$ percentage jump from the working point (e.g. 10 [%])
- U_0 the voltage in the working point - either U_{M0} or U_{T0}

This formula has been also used for the signal amplitude calculation during free transient response measurements.

To systematize the free transient response measurements we decided to excite the system by the periodic signal with time period long enough for the transient responses to fade out Fig. 4.7.

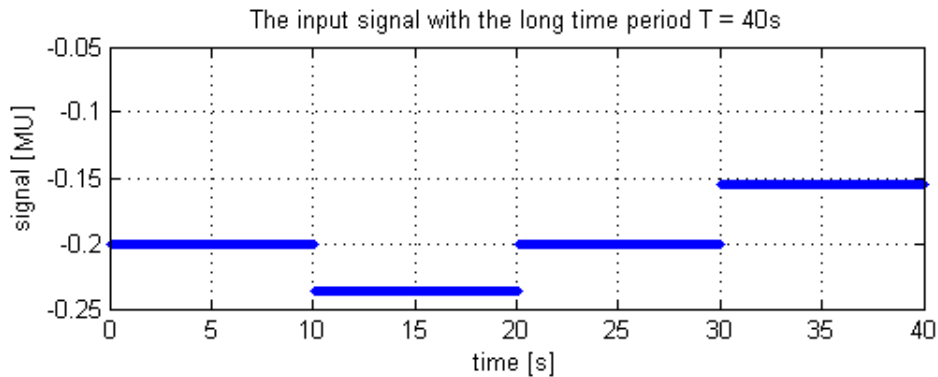


Figure 4.7: Input signal for the measurement of dynamic responses

The regions with the zero deviations are necessary for the system to stabilise in its working point. Each experiment lasts for ten periods i.e.: $T = 400$ seconds. This way we measure the system responses for the several $perc$ [%] jumps from each working point.

The Fig. 4.8 shows the block interconnection for the system identification with holding.

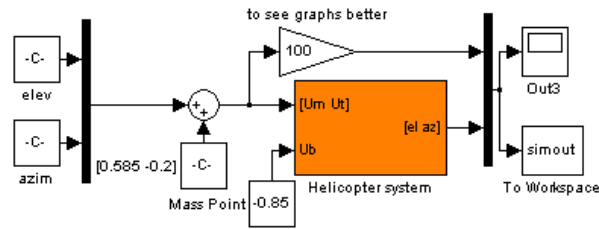


Figure 4.8: The Simulink scheme for the system identification - holding

The Fig. 4.9 shows the block interconnection for the identification of the system dynamics in azimuth.

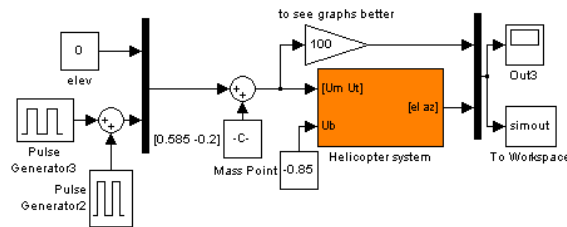


Figure 4.9: The Simulink scheme for the system identification - Azimuth

While fixed azimuth we use the scheme on Fig. 4.9 to identify the coupling dynamics in elevation.

The Fig. 4.10 shows the block interconnection for the identification of the system dynamics in elevation.

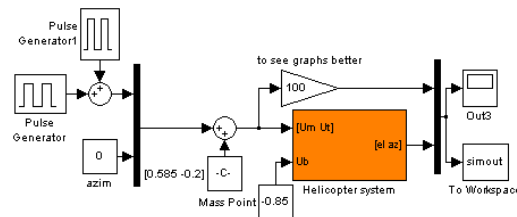


Figure 4.10: The Simulink scheme for the system identification - Elevation

Keeping fixed elevation we use the scheme on Fig. 4.10 to identify the coupling dynamics in azimuth.

4.2.2 Evaluation of step responses with 'holding'

The experiment of the step responses with 'holding' the helicopter assumes that the system is linear so that the **superposition principle** can be applied. It also assumes that the torque applied in the measured axis of rotation is constant.

According to the strategy we described in the chapter 3.2.1 we need to make this measurement very accurately because the identification of motors lies upon the result from this experiment.

To eliminate the reaction time of the examiner we decided to consider the starting point of the system response to be the very first deflection point in the direction of the applied torque.

We start measuring the second working point because it is placed in the middle of the linear region of the static characteristics Fig. 4.1. We measure the influence of the tail motor on the dynamics of the system around the vertical axis of rotation keeping the elevation angle fixed.

We examine the step responses in both directions, clockwise and anti-clockwise, for various amplitudes of input signal. To unify the obtained data all amplitudes are scaled to unit step jump Fig. 4.11.

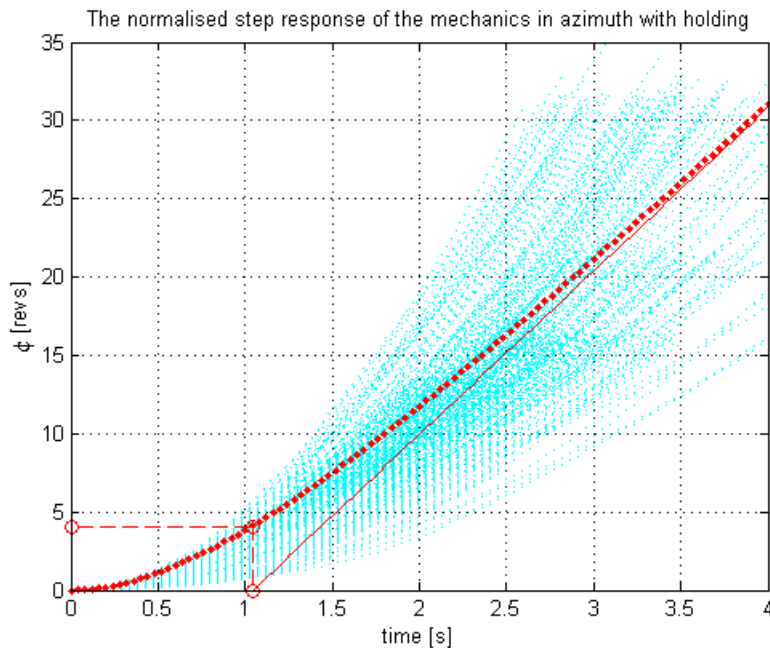


Figure 4.11: The transient response around the vertical axis of rotation,
red - model

We estimated the typical behaviour of the mechanics of the system by calculating the mean values from all obtained results. The parameters of F_{VT} that we achieve are summed up in the Tab. 4.5.

Table 4.5: The F_{VT} identification of working point 2

p_V	$\frac{\kappa_{VT}}{p_T}$
1.03	10.6

4.2.3 Evaluation of free step responses

We continue with the evaluation of the free step responses of the system. We use the information obtained from the experiments that we did with 'holding'.

We examine the step responses in clockwise and anti-clockwise directions for various amplitudes of the input signal and accordingly scale the amplitudes of the output signal Fig. 4.12.

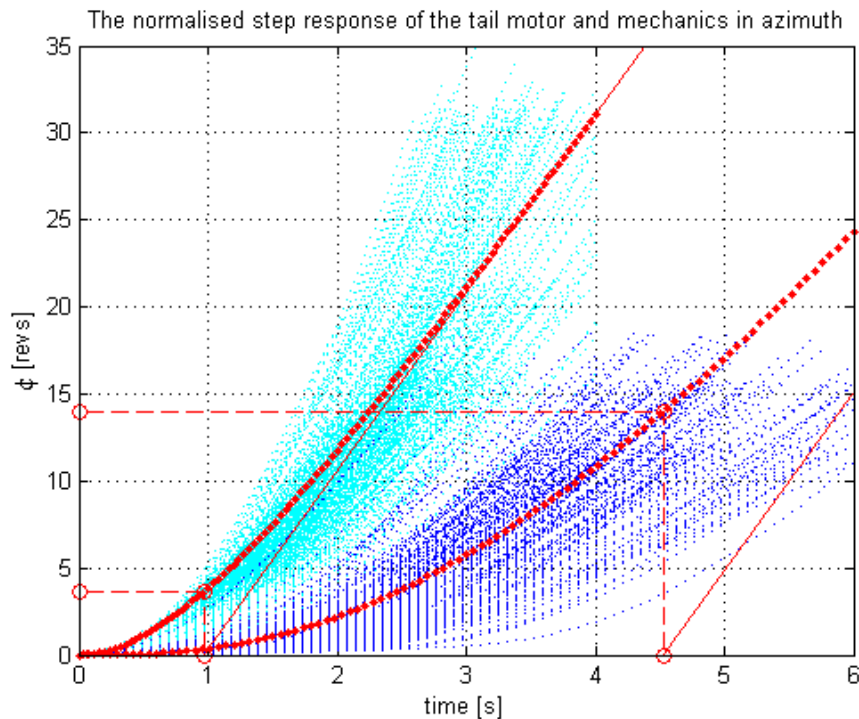


Figure 4.12: Tail motor identification cyan - holding, blue - free, red - model

We estimated the typical dynamics of the system by calculating the mean values from all obtained results. The parameters of G_{VT} we achieve are summed up in the Tab. 4.6.

Table 4.6: The G_{VT} identification of working point 2

p_V	p_T	κ_{VT}
1.03	0.28	2.97

This result is surprising, because according to Tab. 4.6, the dynamics of the tail motor is slower compared to the dynamics of the mechanical parts while we are expecting opposite result. The observed discrepancy might be caused by the reaction time induced by the examiner.

The obtained result has proved that the strategy we were using until now must be reconsidered.

4.2.4 The identification strategy modification

Until now we were trying to identify the dynamics of motors indirectly. This time we identify the dynamics of motor and propeller directly using the apparatus from the steady state spinning rate of motors evaluation experiment described in chapter 4.1.3.

4.2.5 The direct identification of the motors dynamics

The main idea of the direct identification of the motors is based on the equations (2.2) and (2.3). Let us recall the form of that equations:

$$J\dot{\omega}(t) + B\omega(t) = k.U(t) \quad (4.3)$$

We measure step responses in the linear region of the characteristics Fig. 4.4 and Fig. 4.5. The input voltage applied is defined by the following equations

$$\begin{aligned} u(0) &= u_0 = \text{const} \\ u(t > 0) &= u_1 = \text{const} \\ u_1 &\neq u_0 \end{aligned}$$

The solution to equation (4.3) can be derived using e.g. the method of variation of constants:

$$\omega(t) = k \cdot \left(\frac{u_1}{B} + \left(\frac{u_0}{J} - \frac{u_1}{B} \right) \cdot \exp\left(-\frac{B}{J}t\right) \right) \quad (4.4)$$

Substituting $t = \frac{J}{B}$ into (4.4) and rearranging

$$\begin{aligned} \omega\left(\frac{J}{B}\right) &= \left(\frac{k}{B}u_1 - \frac{k}{J}u_0\right)(1 - e^{-1}) + \frac{k}{J}u_0 \\ \omega\left(\frac{J}{B}\right) &= 0.632(\omega(\infty) - \omega(0)) + \omega(0) \end{aligned} \quad (4.5)$$

From the (4.5) we find can estimate the time constant of the motor $t = \frac{J}{B}$. Then the corresponding pole is the inverse value of the time constant:

$$p = \frac{1}{\frac{J}{B}} \quad (4.6)$$

During the steady state spinning rate measurement we were estimating the angular speed of motor by counting the measured pulses over the steady region. To find the transient response of the motor we need to approximate an angular speed of motor from each pulse period. The condition for good results of this experiment is again a very short sampling time.

The time constant of the motor is estimated from the time necessary for the ω to reach 63.2% of the difference between the two steady states as it is shown on the Fig. 4.13 and Fig. 4.14:

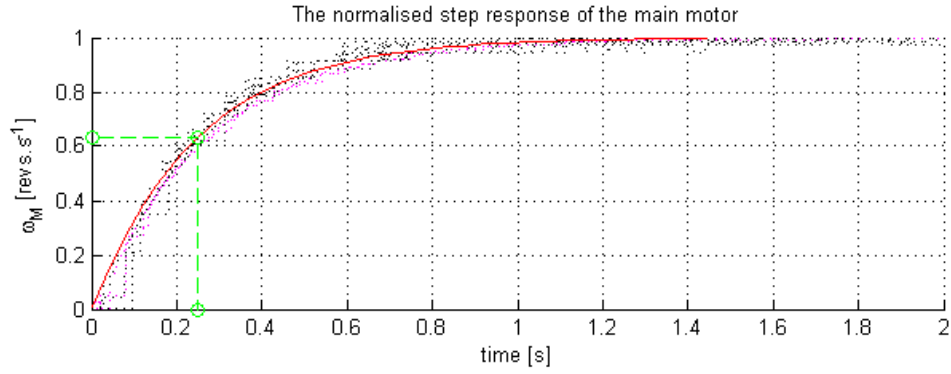


Figure 4.13: Main motor step response, red - model

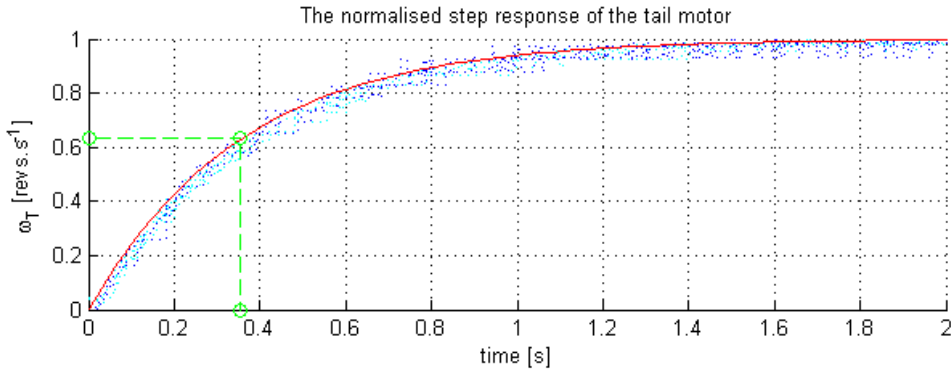


Figure 4.14: Tail motor step response, red - model

Averaging of the obtained parameters and substitution into (3.11) give us Tab. 4.7

Table 4.7: The dynamics of motors

p_T	$\frac{k_T}{J_T}$ [MU]	$\frac{k_T}{J_T}$ [SI]	p_M	$\frac{k_M}{J_M}$ [MU]	$\frac{k_M}{J_M}$ [SI]
2.81	-1087	-1138	4.04	612	320

From the table Tab. 4.7 we conclude that the dynamics of the tail motor is slower than the dynamics of the main motor.

4.2.6 The identification of the first working point

The Fig. 4.15 shows step responses of the system and estimated model.

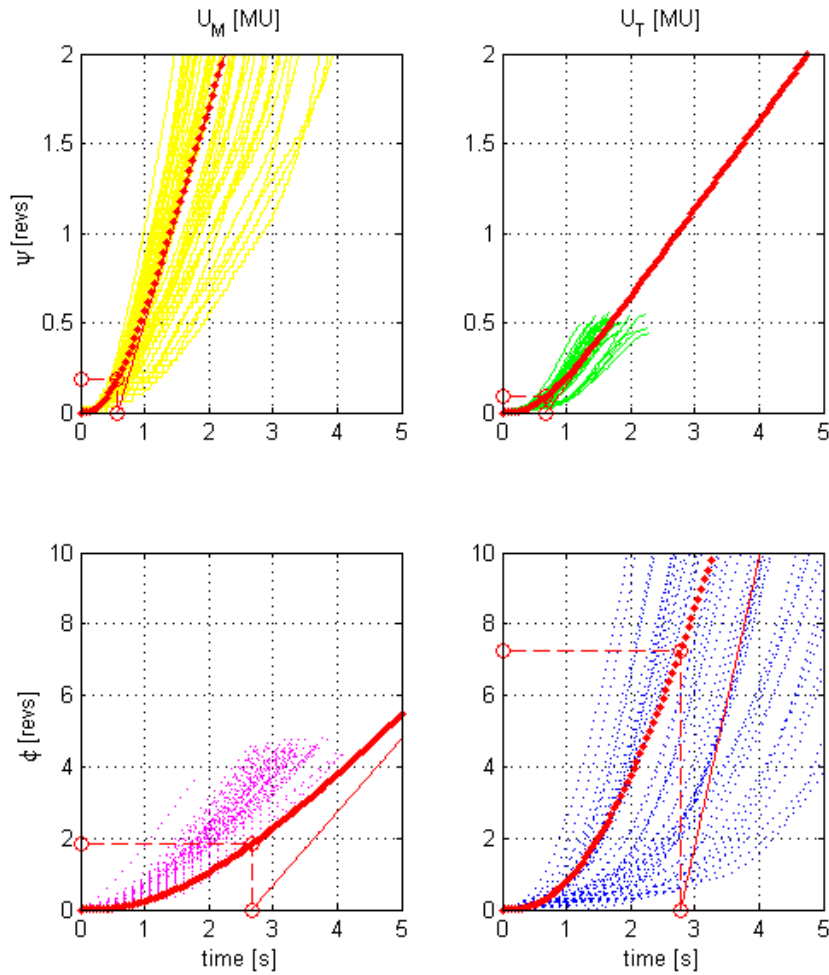


Figure 4.15: Step responses of the system and model(red)

The estimated transfer function in SI units [$\text{rad}\cdot\text{V}^{-1}$] is:

$$\mathbf{G}_1(s) = \begin{pmatrix} G_{HM1} & G_{HT1} \\ G_{VM1} & G_{VT1} \end{pmatrix} = \begin{pmatrix} \frac{7.63}{s(s+3.02)(s+4.04)} & \frac{2.17}{s(s+3.02)(s+2.81)} \\ \frac{1.79}{s(s+0.41)(s+4.04)} & \frac{9.81}{s(s+0.41)(s+2.81)} \end{pmatrix}$$

and Matlab units [$\text{revs}\cdot\text{MU}^{-1}$]:

$$\mathbf{G}_1(s) = \begin{pmatrix} G_{HM1} & G_{HT1} \\ G_{VM1} & G_{VT1} \end{pmatrix} = \begin{pmatrix} \frac{14.6}{s(s+3.02)(s+4.04)} & \frac{4.15}{s(s+3.02)(s+2.81)} \\ \frac{3.42}{s(s+0.41)(s+4.04)} & \frac{9.36}{s(s+0.41)(s+2.81)} \end{pmatrix}$$

4.2.7 The identification of the second working point

The Fig. 4.16 shows step responses of the system and estimated model.

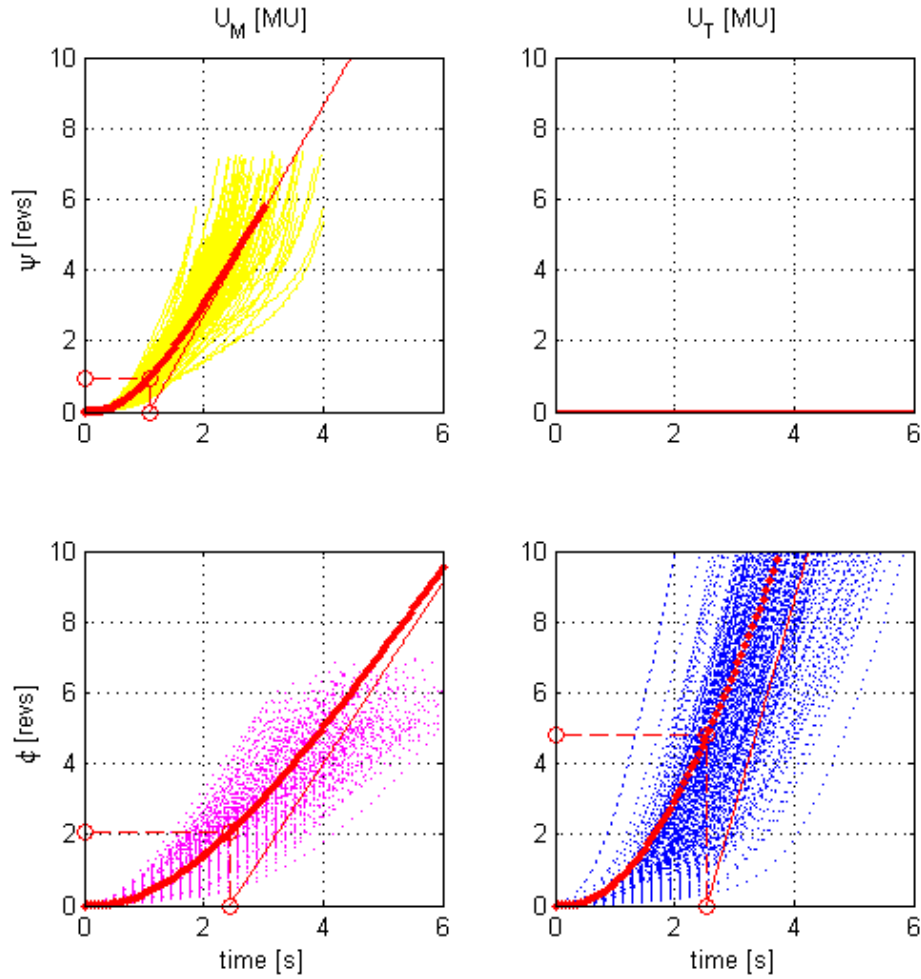


Figure 4.16: Step responses of the system and model(red)

The estimated transfer function in SI units [$\text{rad}\cdot\text{V}^{-1}$] is:

$$\mathbf{G}_2(s) = \begin{pmatrix} G_{HM2} & G_{HT2} \\ G_{VM2} & G_{VT2} \end{pmatrix} = \begin{pmatrix} \frac{7.48}{s(s+1.19)(s+4.04)} & \frac{0.01}{s(s+1.19)(s+2.81)} \\ \frac{2.47}{s(s+0.46)(s+4.04)} & \frac{7.93}{s(s+0.46)(s+2.81)} \end{pmatrix}$$

and Matlab units [$\text{revs}\cdot\text{MU}^{-1}$]:

$$\mathbf{G}_2(s) = \begin{pmatrix} G_{HM2} & G_{HT2} \\ G_{VM2} & G_{VT2} \end{pmatrix} = \begin{pmatrix} \frac{14.3}{s(s+1.19)(s+4.04)} & \frac{0.01}{s(s+1.19)(s+2.81)} \\ \frac{4.73}{s(s+0.46)(s+4.04)} & \frac{7.57}{s(s+0.46)(s+2.81)} \end{pmatrix}$$

4.2.8 The identification of the third working point

The Fig. 4.17 shows steps responses of the system and estimated model.

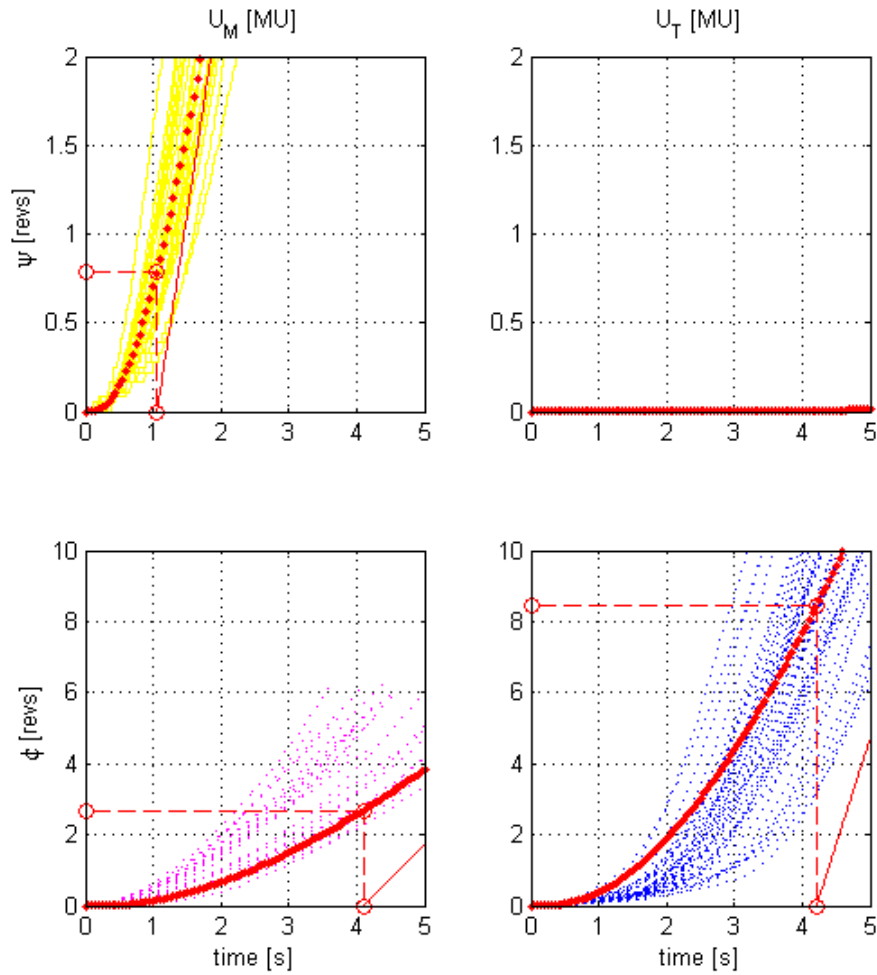


Figure 4.17: Step responses of the system and model(red)

The estimated transfer function in SI units [rad.V^{-1}]:

$$\mathbf{G}_3(s) = \begin{pmatrix} G_{HM3} & G_{HT3} \\ G_{VM3} & G_{VT3} \end{pmatrix} = \begin{pmatrix} \frac{6.59}{s(s+1.24)(s+4.04)} & \frac{0.01}{s(s+1.24)(s+2.81)} \\ \frac{1.04}{s(s+0.26)(s+4.04)} & \frac{4.53}{s(s+0.26)(s+2.81)} \end{pmatrix}$$

and Matlab units [revs.MU^{-1}]:

$$\mathbf{G}_3(s) = \begin{pmatrix} G_{HM3} & G_{HT3} \\ G_{VM3} & G_{VT3} \end{pmatrix} = \begin{pmatrix} \frac{12.6}{s(s+1.24)(s+4.04)} & \frac{0.01}{s(s+1.24)(s+2.81)} \\ \frac{1.99}{s(s+0.26)(s+4.04)} & \frac{4.33}{s(s+0.26)(s+2.81)} \end{pmatrix}$$

Chapter 5

Control Synthesis

5.1 Classical Control Theory

Throughout this chapter we assume that the system is controlled by negative feedback as it is shown on the Fig. 5.1

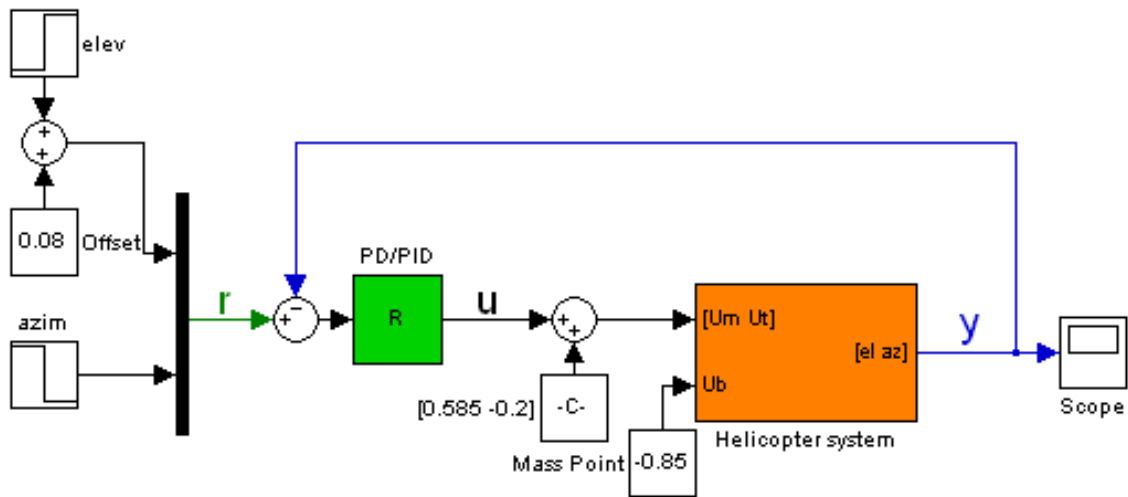


Figure 5.1: The feedback control scheme

5.1.1 Decoupling

To understand the role of the decoupling we need to define an autonomous controller.

Definition 5.1 (autonomous controller): We call MIMO controller autonomous if each output signal is affected by single control signal. ▶

It is evident that to obtain an autonomous control we need at least the same amount of control signals as output signals.

The definition 5.1 implies that the transfer matrix of the closed loop system $\mathbf{F}(s)$ must be diagonal i.e.:

$$\mathbf{F}(s) = (\mathbf{I} + \mathbf{G}(s) \cdot \mathbf{R}(s))^{-1} \mathbf{G}(s) \cdot \mathbf{R}(s) = (\mathbf{I} + \mathbf{H}(s))^{-1} \mathbf{H}(s)$$

- $\mathbf{F}(s)$ the closed loop transfer matrix
- $\mathbf{G}(s)$ the transfer matrix of the system
- $\mathbf{R}(s)$ the transfer matrix of the controller
- $\mathbf{H}(s)$ the open loop transfer matrix
- \mathbf{I} the unity matrix of the corresponding size

We see that to ensure the diagonality of the closed loop system $\mathbf{F}(s)$ the open loop transfer function $\mathbf{H}(s)$ must be diagonal. (we skip the (s) notation)

$$\mathbf{H} = \begin{pmatrix} H_{HM} & 0 \\ 0 & H_{VT} \end{pmatrix} = \begin{pmatrix} G_{HM} & G_{HT} \\ G_{VM} & G_{VT} \end{pmatrix} \cdot \begin{pmatrix} R_{HM} & R_{HT} \\ R_{VM} & R_{VT} \end{pmatrix} \quad (5.1)$$

Therefore the adjacent transfer functions of the controller are defined

$$R_{HT} = -R_{VT} \frac{G_{HT}}{G_{HM}} \quad R_{VM} = -R_{HM} \frac{G_{VM}}{G_{VT}} \quad (5.2)$$

In the case of our helicopter we may use the following substitution

$$S_{HT} = \frac{G_{HT}}{G_{HM}} = \frac{\kappa_{HT}}{\kappa_{HM}} \frac{(s + p_T)}{(s + p_M)}$$

$$S_{VM} = \frac{G_{VM}}{G_{VT}} = \frac{\kappa_{VM}}{\kappa_{VT}} \frac{(s + p_M)}{(s + p_T)}$$

Then the (5.2) will gain following form

$$R_{HT} = -R_{VT} \cdot S_{HT} \quad R_{VM} = -R_{HM} \cdot S_{VM} \quad (5.3)$$

Substituting (5.2) back to (5.1)

$$H_{HT} = \left(G_{HM} - \frac{G_{HT} \cdot G_{VM}}{G_{VT}} \right) \cdot R_{HM}$$

$$H_{VT} = \left(G_{VT} - \frac{G_{HT} \cdot G_{VM}}{G_{HM}} \right) \cdot R_{VT}$$

Therefore to decouple the cross bond between the main propeller and azimuth angle we will need to design the controllers R_{HM} and R_{VT} for the transfer functions:

$$S_{HM} = G_{HM} - \frac{G_{HT} \cdot G_{VM}}{G_{VT}} = \frac{\kappa_{HM} - \frac{\kappa_{HT} \kappa_{VM}}{\kappa_{VT}}}{s(s + p_H)(s + p_M)} \quad (5.4)$$

$$S_{VT} = G_{VT} - \frac{G_{HT} \cdot G_{VM}}{G_{HM}} = \frac{\kappa_{VT} - \frac{\kappa_{HT} \kappa_{VM}}{\kappa_{HM}}}{s(s + p_V)(s + p_T)} \quad (5.5)$$

To complete the control design we find the remaining controllers R_{HT} and R_{VM} from (5.3).

5.1.2 Frequency methods for PD control design

The frequency design methods are well known and the rigorous derivation of the control design is described in (JOHN, J., 1996, page 36) or (FRANKLIN, G.F., POWEL, J.D., EMAMI-NAEINI, A., 2006, page 353).

We decided to design a proportional-derivation 'PD' controller to speed up the transient responses of the system. Both S_{HM} and S_{VT} contain pure integrators, therefore if tests with the helicopter system prove that the system quickly diminishes the steady state error we will not need to design proportional-integral-derivative PID controllers.

We follow the design procedure to obtain the PD controller with a specific **phase margin (PM)**. The phase margin is an amount by which the phase of the open loop system $H(j\omega)$ exceeds -180° when the gain $|K.H(j\omega)| = 1$. The phase margin defines the stability of a closed loop.

We firstly design the pure PD controller of the form:

$$R^*(s) = r_d \cdot s + r_p$$

Because pure PD controller is not realisable by means of physical elements we design a **lead compensated** PD controller adding a first-order pole to the derivative component r_d in order to alleviate the high-frequency amplification of the pure PD control.

$$R(s) = \frac{r_d \cdot s}{\frac{r_d \cdot s}{N} + 1} + r_p$$

The N is the lead ratio. The role of the lead ratio is clearly seen from the initial value of the step response of the controller.

$$\begin{aligned} u(0) &= \lim_{t \rightarrow 0} r(t) = \lim_{s \rightarrow \infty} r(s) \cdot s \cdot R(s) = \lim_{s \rightarrow \infty} \frac{s}{s} R(s) = \\ &= \lim_{s \rightarrow \infty} \frac{r_d \cdot s}{\frac{r_d \cdot s}{N} + 1} + r_p = \lim_{s \rightarrow \infty} \frac{s(N + r_p) + \frac{N}{r_d} r_p}{s + \frac{N}{r_d}} = N + r_p \end{aligned}$$

We see that the main purpose of the lead ratio is to set a ceiling to the initial peak value of the control response $u(0)$ with the minimal influence to all other parameters of the pure PD controller.

To avoid the overloading of the actuators we usually set the lead ratio $N=10$.

We show the design procedure of the PD controller for the phase margin $PM = 60^\circ$ for the transfer function S_{HM} of the first working point.

$$S_{HM} = \frac{13.1}{s(s + 3.02)(s + 4.04)}$$

The Fig. 5.2 shows the Bode plots for the pure PD design.

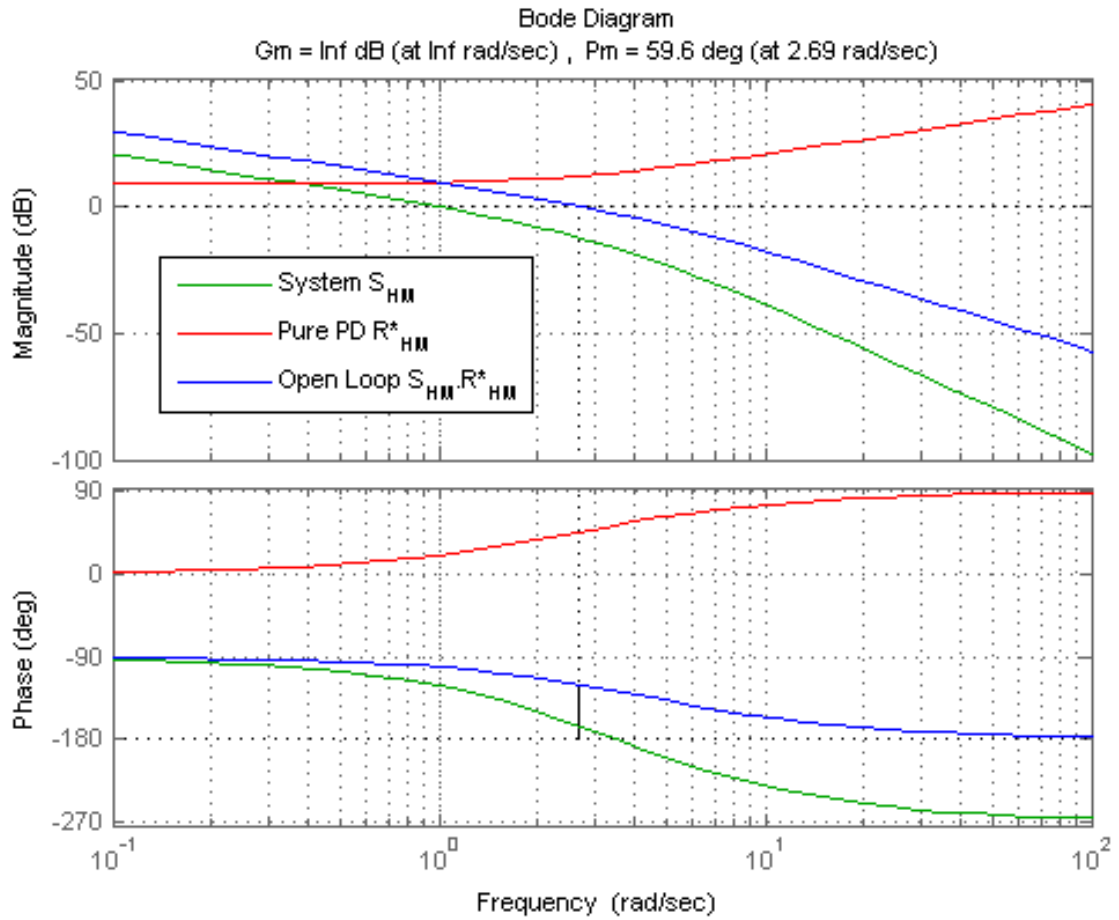


Figure 5.2: Pure PD controller design - frequency methods

The obtained controller is in the form:

$$R^*_{HM} = 1.06s + 2.85$$

The Fig. 5.3 shows the Bode plots for the lead compensated PD controller (N=20).

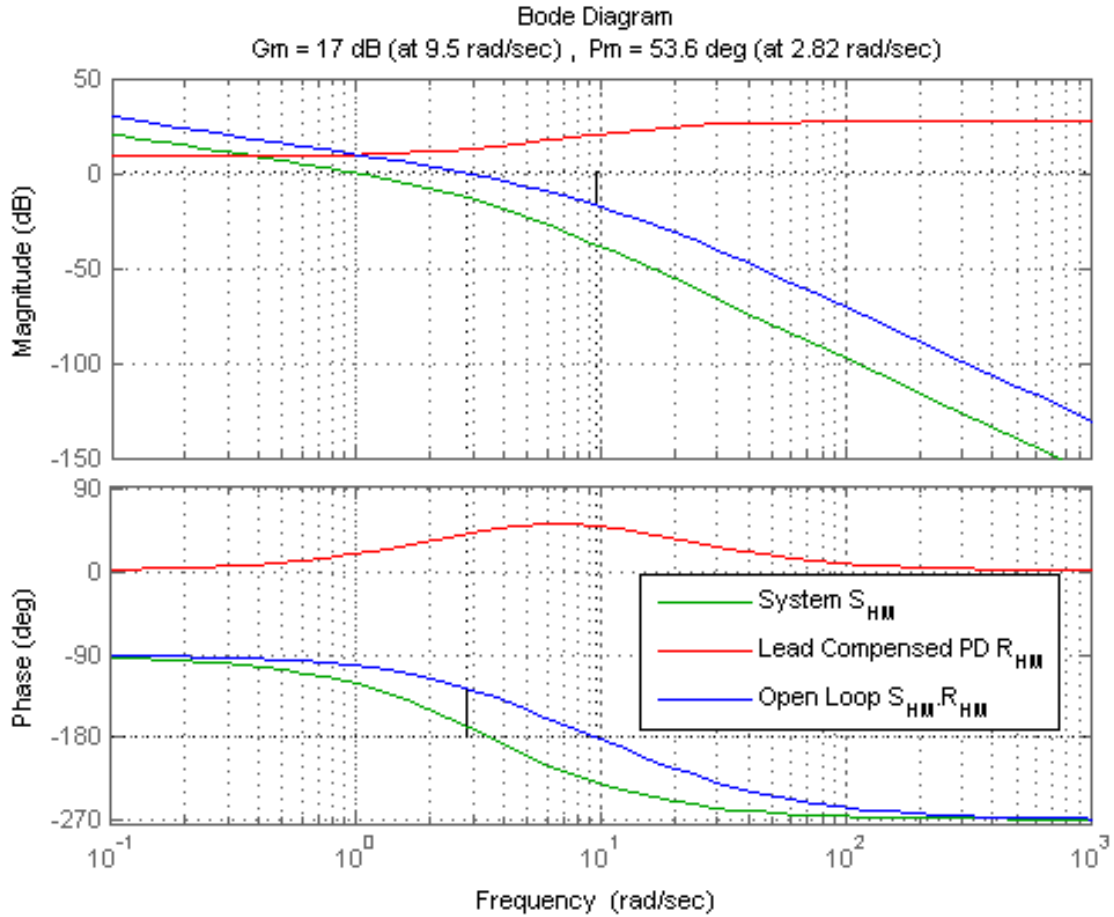


Figure 5.3: Lead compensated PD controller design - frequency methods

$$R_{HM} = \frac{24.2s + 57}{1.06s + 20}$$

In the same fashion we obtain the PD controller for the S_{VT} with the phase margin $PM = 30^\circ$.

$$S_{VT} = \frac{8.4}{s(s + 0.41)(s + 2.81)}$$

The lead compensated transfer function R_{VT} for N=10:

$$R_{VT} = \frac{4.7s + 6.9}{0.44s + 10}$$

The Fig. 5.4 compares the expected and measured step responses of the system.

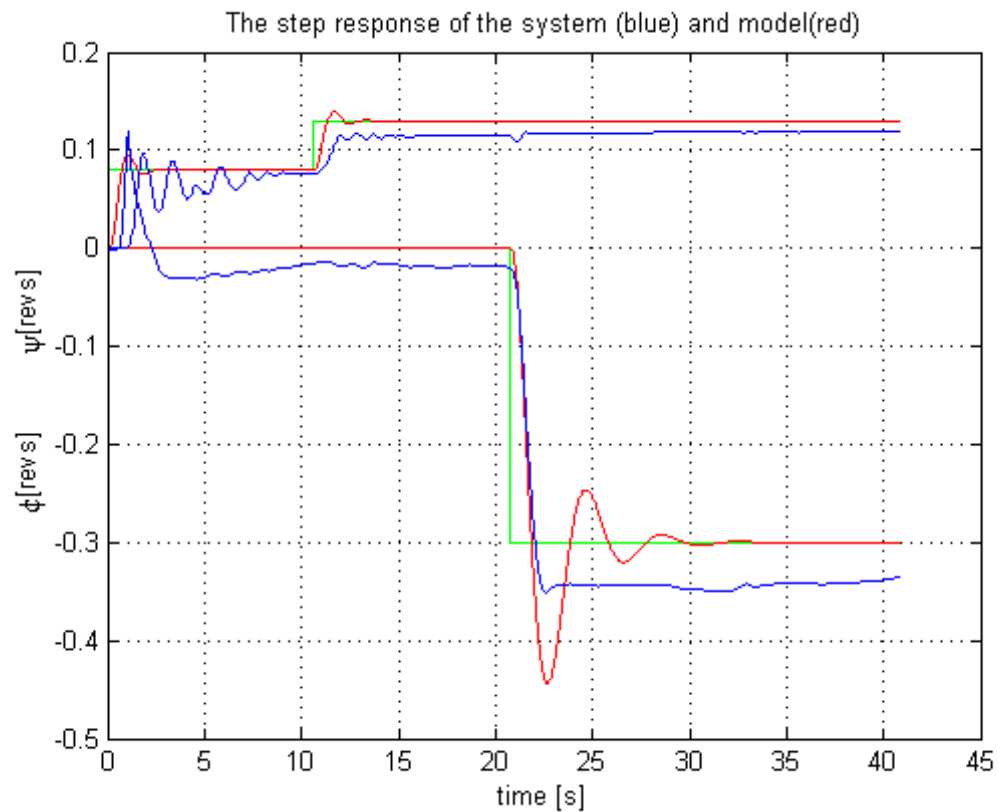


Figure 5.4: The comparison of the system and model step responses

From the Fig. 5.4 we conclude that the controller diminishes the steady state error very slowly, therefore we need to design PID controllers.

5.1.3 Frequency methods for PID control design

We show the design procedure of the proportional-integral-derivative PID controller for the phase margin $PM = 20^\circ$ for the transfer function S_{VT} of the first working point.

The Fig. 5.5 shows the Bode plots for the lead compensated PID controller ($N=10$).

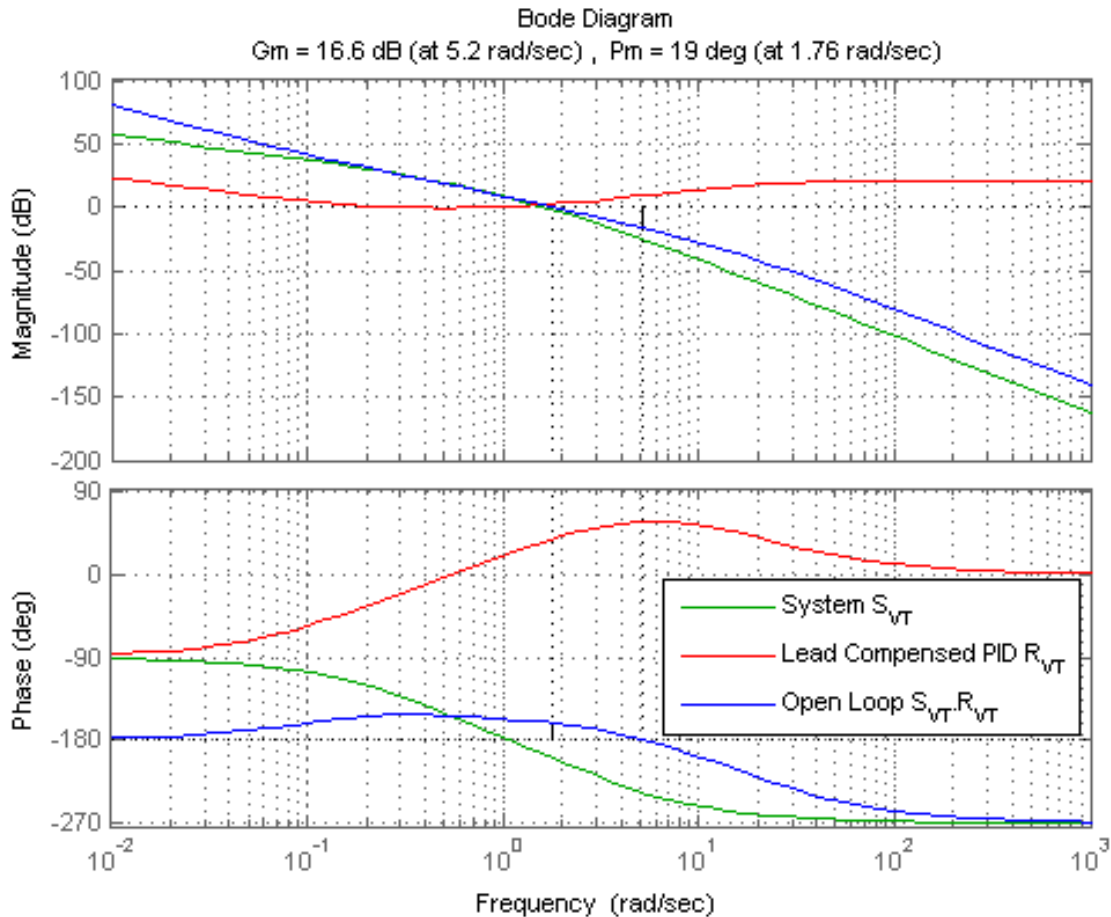


Figure 5.5: Lead compensated PID controller design - frequency methods

The lead compensated transfer function of the R_{VT} for $N=10$:

$$R_{VT} = \frac{5.34s^2 + 9.3s + 1.44}{0.49s^2 + 10s}$$

The lead compensated transfer function of the R_{HM} for phase margin $PM=60$ and $N=20$:

$$R_{HM} = \frac{21.9s^2 + 51.3s + 10.9}{0.97s^2 + 20s}$$

The Fig. 5.6 shows the step responses of the closed loop system.

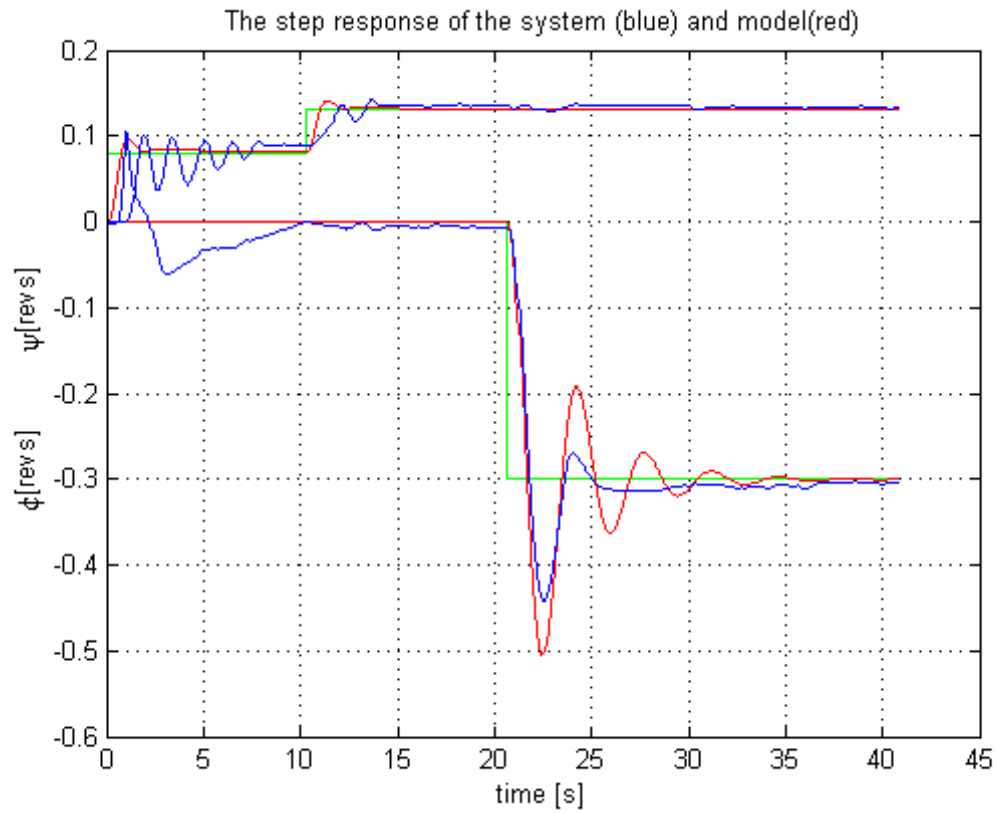


Figure 5.6: The comparison of the system and model step responses

If we compare the Fig. 5.6 with Fig. 5.4 we see that the system reacts quickly and diminishes the steady state error. The interesting fact to notice is that in the both systems there is no coupling.

The Fig. 5.7 shows the step responses of the closed loop system with coupling.

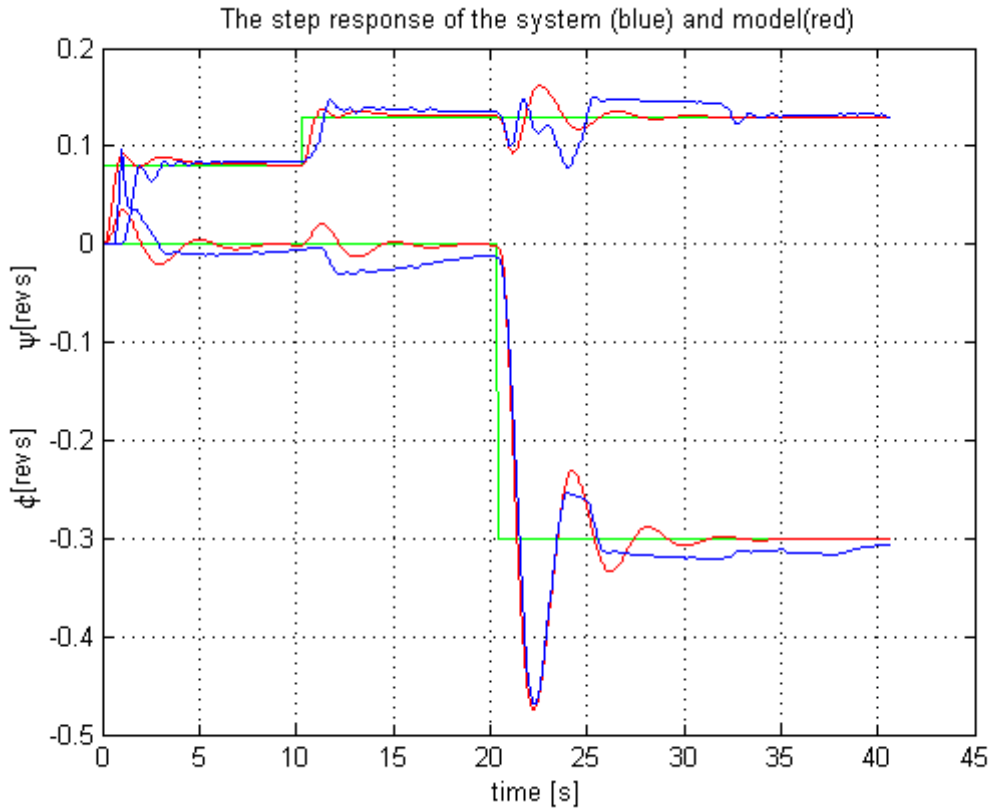


Figure 5.7: The comparison of the system and model step responses - coupling

We can see that in the time interval from 10 to 15 seconds both azimuth and elevation react on the change in elevation. The same phenomenon occurs in the time interval from 20 to 25 second where both angles are affected by the change in the azimuth angle.

The Fig. 5.7 has been achieved when we put the R_{HT} and R_{VM} equal to zero.

5.1.4 Root locus methods for PID control design

The root locus design techniques are also well known and the rigorous design description can be found in (JOHN, J., 1996, page 21) or (FRANKLIN, G.F., POWEL, J.D., EMAMI-NAEINI, A., 2006, page 230).

During the root locus design we use the `rltool` in Matlab.

We show the design procedure of the PID controller for the transfer function S_{HM} of the third working point.

$$S_{HM} = \frac{12.6}{s(s + 1.24)(s + 4.04)}$$

We set two design criteria. The first is the **settling time** has to be less than 5 seconds. The last criterion is the **fitst overshoot** has to be less than 30%.

The Fig. 5.8 shows the resultant pole location.

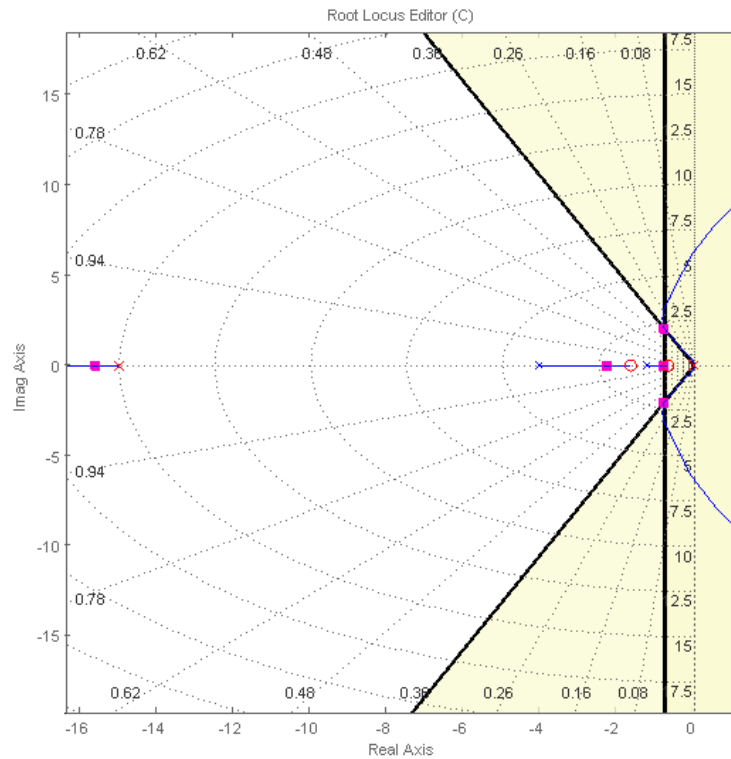


Figure 5.8: The root locus of the S_{HM}

The obtained transfer function is:

$$R_{HM} = \frac{9.62(s + 0.7)(s + 1.6)}{s(s + 15)}$$

We apply the same design criteria to find the PD controller for S_{VT} .

$$S_{VT} = \frac{4.33}{s(s + 0.26)(s + 2.81)}$$

The Fig. 5.9 shows the resultant pole location.

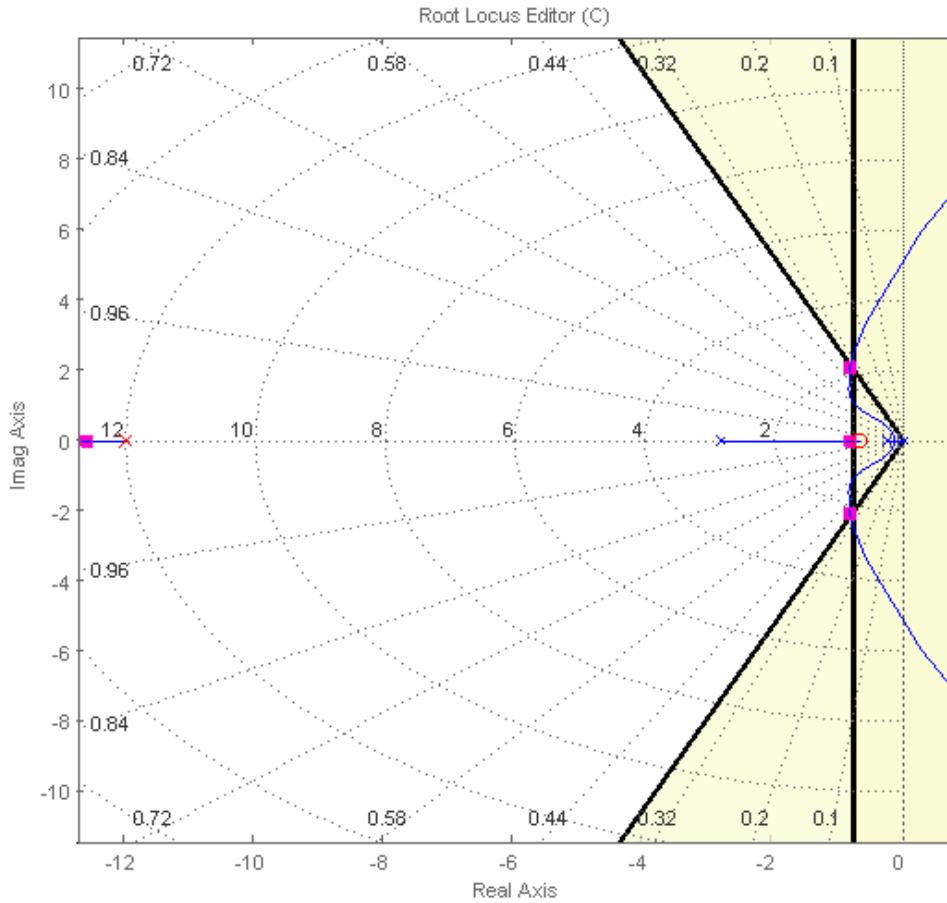


Figure 5.9: The root locus of the S_{VT}

The obtained transfer function is:

$$R_{VT} = \frac{17.5(s + 0.69)}{s + 12}$$

The Fig. 5.10 shows the step responses of the closed loop system.

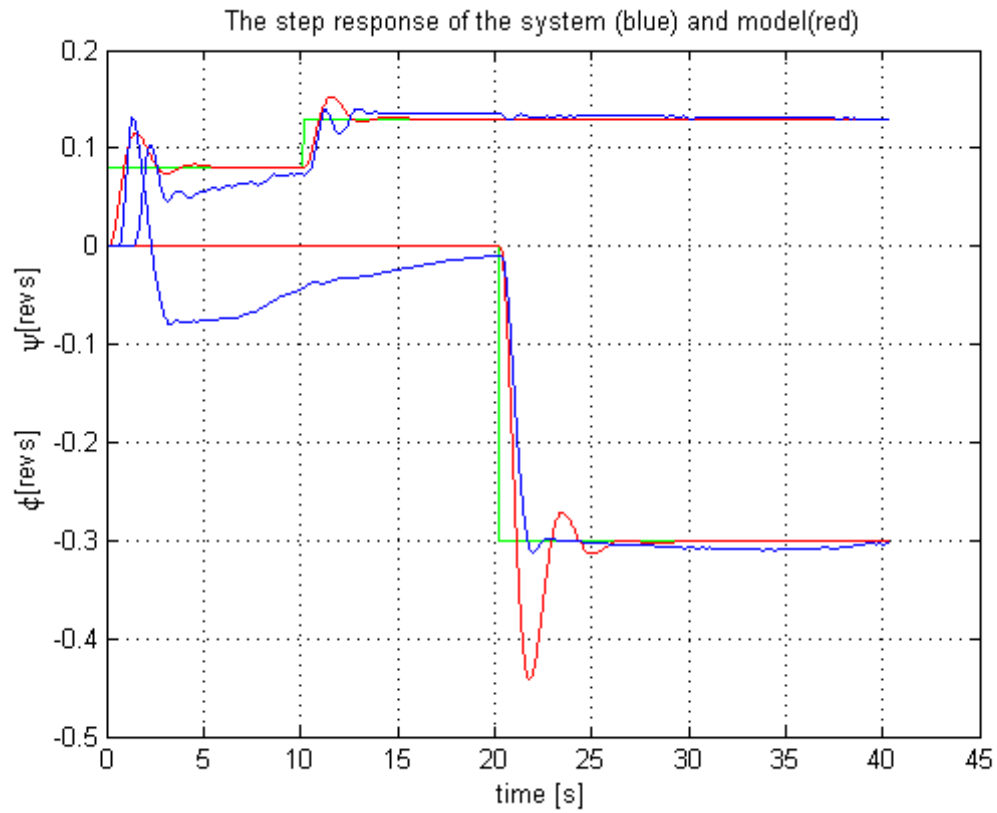


Figure 5.10: The comparison of the system and model step responses

If we compare the Fig. 5.10 with Fig. 5.4 we see that the system reacts quickly and diminishes the steady state error. The first overshoot is lower probably because the identified model has got the greater gain than the real system.

5.2 Modern Control Theory

5.2.1 The discretization of the continuous system

Until now we assumed that the system is continuous. Nevertheless the truth is, that we scan data discretely with a sampling period $T_s = 0.01$ seconds. For the Kalman filter design and following LQG and MPC control design we need to discretize our plant.

We use the zero order hold - Evans discretization method implemented in Matlab as `c2d` which is described in the (HAVLENA, V., ŠTECHA, J., 2000, page 19).

We decided to show the control design procedure on the system set in the second working point.

$$\mathbf{A} = \begin{pmatrix} -4.04 & 0 & 0 & 0 & 0 & 0 \\ 0 & -2.81 & 0 & 0 & 0 & 0 \\ 0.003 & -0.004 & -0.46 & 0 & 0 & 0 \\ 0.012 & -0.00 & 0 & -1.56 & 0 & 0 \\ 0 & 0 & 0 & 1 & 0 & 0 \\ 0 & 0 & 1 & 0 & 0 & 0 \end{pmatrix} \quad \mathbf{B} = \begin{pmatrix} 612 & 0 \\ 0 & -1087 \\ 0 & 0 \\ 0 & 0 \\ 0 & 0 \\ 0 & 0 \end{pmatrix}$$

$$\mathbf{C} = \begin{pmatrix} 0 & 0 & 0 & 0 & 1 & 0 \\ 0 & 0 & 0 & 0 & 0 & 1 \end{pmatrix} \quad \mathbf{D} = \begin{pmatrix} 0 & 0 \\ 0 & 0 \end{pmatrix}$$

Substituting into ($T_s = 0.01s$):

$$\mathbf{A}_d = e^{\mathbf{A}T_s} \quad \mathbf{B}_d = e^{\mathbf{A}T_s} \int_0^{T_s} e^{-\mathbf{A}\tau} d\tau \mathbf{B}$$

we obtain:

$$\mathbf{A}_d = \begin{pmatrix} 0.96 & 0 & 0 & 0 & 0 & 0 \\ 0 & 0.97 & 0 & 0 & 0 & 0 \\ 0.00 & -0.00 & 0.99 & 0 & 0 & 0 \\ 0.00 & -0.00 & 0 & 0.98 & 0 & 0 \\ 0.00 & -0.00 & 0 & 0.01 & 0 & 0 \\ 0.00 & -0.00 & 0.01 & 0 & 0 & 0 \end{pmatrix} \quad \mathbf{B}_d = \begin{pmatrix} 5.99 & 0 \\ 0 & -10.7 \\ 0.00 & 0.00 \\ 0.00 & 0.00 \\ 0.00 & 0.00 \\ 0.00 & 0.00 \end{pmatrix}$$

$$\mathbf{C} = \begin{pmatrix} 0 & 0 & 0 & 0 & 1 & 0 \\ 0 & 0 & 0 & 0 & 0 & 1 \end{pmatrix} \quad \mathbf{D} = \begin{pmatrix} 0 & 0 \\ 0 & 0 \end{pmatrix}$$

We see that the discretized system is also asymptotically stable and reachable (all its unstable modes are detectable).

Before we proceed to the Kalman filter design we have to examine the observability of the system. The system is observable if:

$$\text{rank} \begin{bmatrix} \mathbf{C} \\ \mathbf{C}.\mathbf{A} \\ \vdots \\ \mathbf{C}.\mathbf{A}^{N-1} \end{bmatrix} = N$$

where N is the order of the system.

Substituting into the previous equation we realize that this condition is fulfilled and the obtained discretized system is observable.

5.2.2 Kalman filter design

Lets assume the linearized discrete system:

$$\begin{aligned} x(k+1) &= \mathbf{A}_d x(k) + \mathbf{B}_d u(k) + v(k) \\ y(k) &= \mathbf{C} x(k) + \mathbf{D} u(k) + e(k) \end{aligned}$$

where $v(k)$ and $e(k)$ are the disturbance (process noise) and measurement noise respectively, which we assume to be uncorrelated zero-mean Gaussian stochastic with constant power spectral density matrices:

$$\mathbf{E} \left\{ \begin{bmatrix} v(k_1) \\ e(k_1) \end{bmatrix} \begin{bmatrix} v(k_2) \\ e(k_2) \end{bmatrix}^T \right\} = \begin{bmatrix} \mathbf{Q} & \mathbf{O} \\ \mathbf{O} & \mathbf{R} \end{bmatrix} \delta(k_1 - k_2)$$

where δ is the Dirac function.

If we restrict ourselves on suboptimal solution, then the Kalman filter has the structure of an ordinary state estimator or observer:

$$\hat{x}(k+1) = \mathbf{A}_d \hat{x}(k) + \mathbf{B}_d u(k) + \mathbf{L} (y - \mathbf{C} \hat{x})$$

where \hat{x} is the estimated state vector and \mathbf{L} is a Kalman gain.

The suboptimal solution of \mathbf{L} which minimizes

$$\mathbf{P}(k) = \mathbf{E} \left\{ [x(k) - \hat{x}(k)]^T [x(k) - \hat{x}(k)] \right\}$$

is defined by the steady state solution of the Riccati equation

$$\begin{aligned} \mathbf{P}(k+1|k) &= \mathbf{A}_d \mathbf{P}(k|k-1) \mathbf{A}_d^T + \mathbf{Q} - \mathbf{L}(k) \mathbf{C} \mathbf{P}(k|k-1) \mathbf{A}_d^T \\ \mathbf{L}(k) &= \mathbf{A}_d \mathbf{P}(k|k-1) \mathbf{C}^T (\mathbf{C} \mathbf{P}(k|k-1) \mathbf{C}^T + \mathbf{R})^{-1} \end{aligned}$$

where \mathbf{Q} and \mathbf{R} represent the cost matrices.

To find the Kalman gain we use the Matlab function `kalman` with parameters

$$\mathbf{Q} = \mathbf{I}$$

$$\mathbf{R} = \mathbf{I}$$

The Fig. 5.11 shows the interconnection of the Kalman filter. For the simplicity we set $\mathbf{D} = 0$.

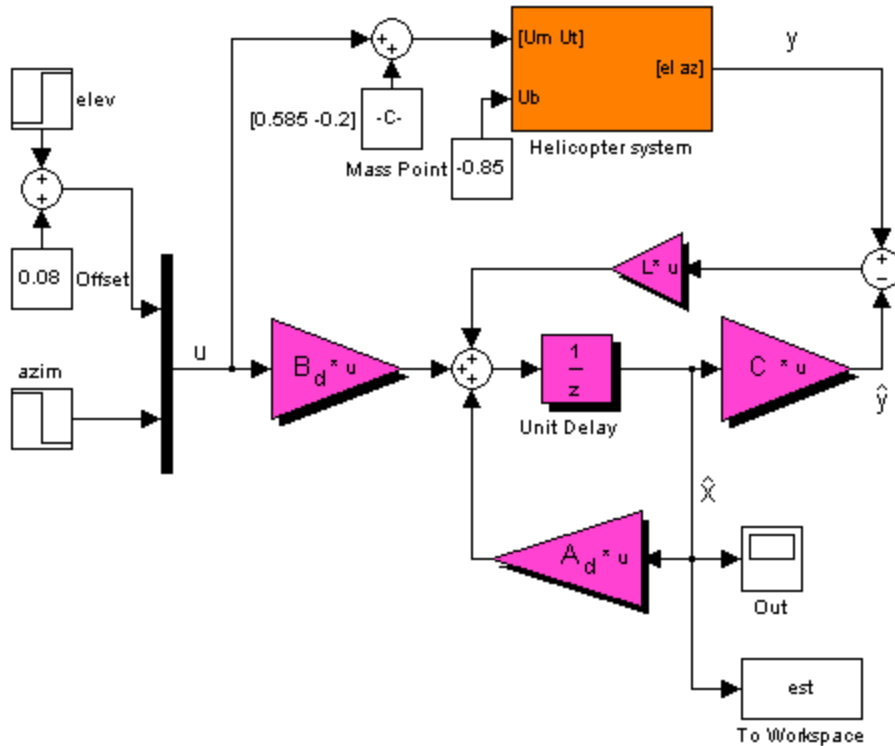


Figure 5.11: The Kalman filter Simulink scheme

The Fig. 5.12 shows the step responses of the closed loop system with PID control. States are monitored by the Kalman filter. The important fact to mention is that the Fig. 5.12 shows **deflections of the states** from the working point.

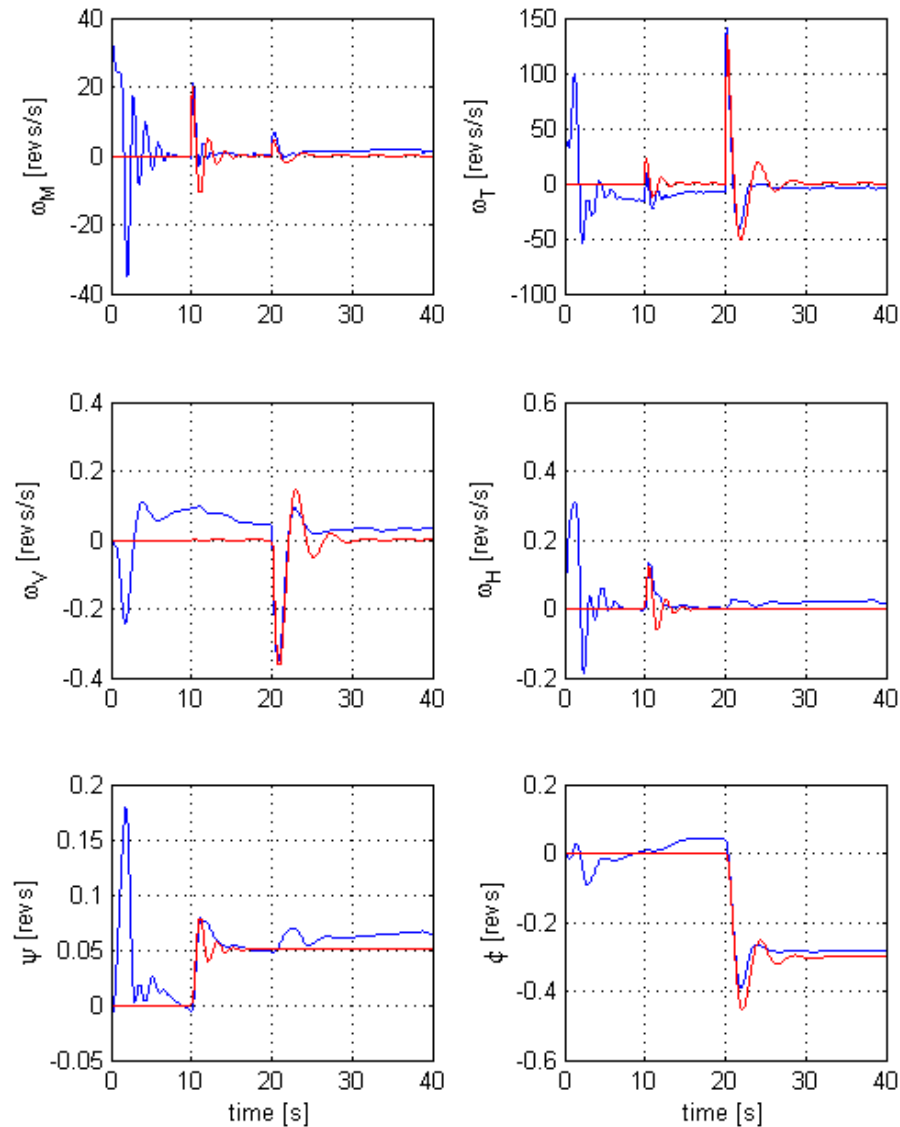


Figure 5.12: The comparison of the estimated states (blue) and model(red)

From the Fig. 5.12 we see that the estimated states are quickly convergent. For the LQG and MPC design we can substitute last two estimated states directly by the measured output signal. This substitution will increase the accuracy of the controller.

5.2.3 LQG control design

'The name LQG arises from the use of a Linear model, an integral Quadratic cost function, and Gaussian white noise processes to model disturbance signals and noise.'

(SKOGESTAD, S., POSTLETHWAITE, I., 2003, page 345).

Let us assume linear discrete dynamic system in the form:

$$\begin{aligned}x(k+1) &= \mathbf{A}_d \cdot x(k) + \mathbf{B}_d \cdot u(k) \\y(k) &= \mathbf{C} \cdot x(k) + \mathbf{D} \cdot u(k)\end{aligned}\tag{5.6}$$

The LQG control problem is to find out the optimal control $\mathbf{u}(\mathbf{k})$ which minimizes:

$$J = \frac{1}{2} x^T(N) \mathbf{Q}(N) x(N) + \frac{1}{2} \sum_{k=t_0}^{N-1} \begin{bmatrix} x^T(k) & u^T(k) \end{bmatrix} \begin{bmatrix} \mathbf{Q}(k) & \mathbf{O} \\ \mathbf{O} & \mathbf{R}(k) \end{bmatrix} \begin{bmatrix} x(k) \\ u(k) \end{bmatrix}\tag{5.7}$$

where t_0 is the initial time and the N is the final time. Matrices \mathbf{Q} and \mathbf{R} are representing cost functions. Minimizing the criterion (5.7) we obtain the Ricatti equation:

$$\mathbf{P}(k) = \mathbf{Q} + \mathbf{A}_d^T \cdot \mathbf{P}(k+1) \mathbf{M} - \mathbf{A}_d^T \cdot \mathbf{P}(k+1) \mathbf{B}_d \cdot \mathbf{K}(k)$$

where $\mathbf{K}(k)$ is the Kalman gain

$$\mathbf{K}^T(k) = (\mathbf{R} + \mathbf{B}_d^T \mathbf{P}(k+1) \mathbf{B}_d)^{-1} \mathbf{B}_d \mathbf{P}(k+1) \mathbf{A}_d$$

the optimal control is then equal to

$$\mathbf{u}^*(k) = -\mathbf{K}^T(k) \cdot x(k)$$

To find out the Kalman gain we use `dlqr` function implemented in Matlab with the cost matrices:

$$\begin{aligned}\mathbf{Q} &= (\text{diag}([100 \ 100 \ 1 \ 1 \ 0.01 \ 0.1]))^{-2} \\ \mathbf{R} &= \text{diag}([1 \ 1])\end{aligned}$$

The Fig. 5.14 shows the step responses of the closed loop system with LQG control.

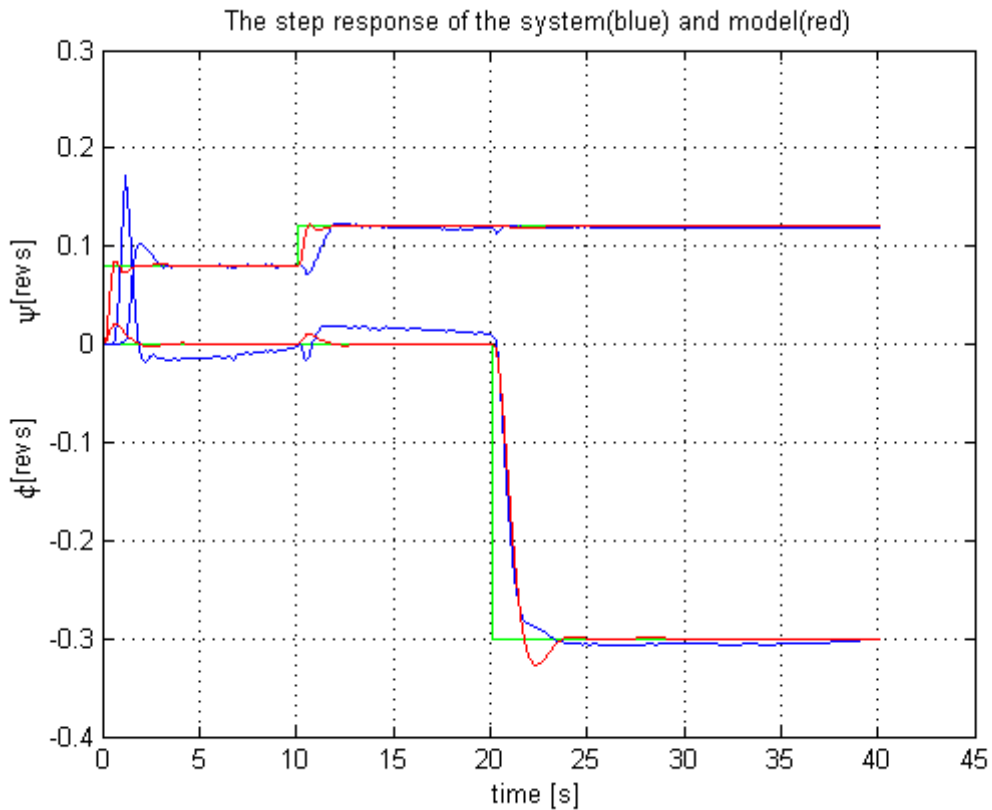


Figure 5.14: The comparison of the system and model step responses

As we expect the LQG performance with the PID is better in the sense of minimal overshoot and settling time. The interesting fact to notice is the coupling which is clearly visible in the time interval from 10 to 15 seconds. The coupling can be gradually diminished by iterative optimization of the \mathbf{Q} and \mathbf{R} matrices.

During the time interval from 10 to 20 seconds we see that the LQG slowly diminished the steady state error in azimuth. This can be further improved by introducing the integral component into the azimuth control.

5.2.4 Model Predictive Control (MPC) design

The rigorous derivation of the model predictive control for the SISO systems is well described in (ROUBAL, J. et al., 2005, page 55).

We will find a receding horizon control MPC for the discretized system (5.6) that minimizes:

$$J = \sum_{k=0}^{T_p-1} \{ \mathbf{q}[y(k) - w(k)]^2 + \mathbf{r}[u(k)]^2 \} \quad (5.8)$$

where T_p is the prediction horizon, \mathbf{q} and \mathbf{r} are cost matrices, $w(k)$ is the reference signal.

The system response to the reference signal is:

$$\begin{bmatrix} y(0) \\ y(1) \\ y(2) \\ \vdots \\ y(T_p - 1) \end{bmatrix} = \begin{bmatrix} \mathbf{C} \\ \mathbf{C}\mathbf{A}_d \\ \mathbf{C}\mathbf{A}_d^2 \\ \vdots \\ \mathbf{C}\mathbf{A}_d^{T_p-1} \end{bmatrix} x(0) + \begin{bmatrix} \mathbf{D} & & & & \\ \mathbf{C}\mathbf{B}_d & \mathbf{D} & & & \\ \mathbf{C}\mathbf{A}_d\mathbf{B}_d & \mathbf{C}\mathbf{B}_d & \mathbf{D} & & \\ \vdots & & \ddots & \ddots & \\ \mathbf{C}\mathbf{A}_d^{T_p-2}\mathbf{B}_d & & & \mathbf{C}\mathbf{B}_d & \mathbf{D} \end{bmatrix} \begin{bmatrix} u(0) \\ u(1) \\ u(2) \\ \vdots \\ u(T_p - 1) \end{bmatrix}$$

Rewriting into the matrix form:

$$\mathbf{y} = \mathbf{V}x(0) + \mathbf{S}u = \tilde{\mathbf{y}} + \mathbf{S}u$$

where the $\tilde{\mathbf{y}}$ represents a system response to the initial condition and $\mathbf{S}u$ is a system response to the control sequence on the horizon T_p .

Substituting into (5.8) and rearranging we obtain the control law:

$$u^*(k) = -\mathbf{N}x(k) + \mathbf{M}w(k)$$

where

$$w(k) = \begin{bmatrix} u_1(k) \\ \vdots \\ u_1(k + T_p - 1) \\ u_2(k) \\ \vdots \\ u_2(k + T_p - 1) \end{bmatrix}$$

We modify the given example Matlab code from (ROUBAL, J. et al., 2005, page 66) such that it is applicable for the MIMO helicopter system.

```
function [M, N, Z, Ab, Bb, Cb, Db] = mympc(Tp, dsys, Q, R)
% MYMPC computes analytical MPC regulator with BUFFER (Ab, Bb, Cb, Db)
% for the discretized system DSYS with 2 inputs and 2 outputs according to
% given prediction horizon Tp(in steps) and weighting matrices Q and R.
%
% USE: [M, N, Z, Ab, Bb, Cb, Db] = mympc(Tp, dsys, Q, R)

[Ad,Bd,Cd,Dd,E,Ts] = dssdata(dsys);
%----- Matrix y~ /x0 for prediction
V = [];
for i = 0 : 1 : Tp-1
    V = [V;Cd*Ad^i];
end
%----- Matrix S for prediction
S = zeros(2*Tp);
S(3:4,1:2)=Cd*Bd;
for i = 3 : 2: 2*Tp-2
    for j = 1 : 2: i
        S(i+2:i+3,j:j+1) = Cd*Ad^((i-j)/2)*Bd;
    end
end
%----- Matrices for analytical MPC controller
G = inv(S'*Q*S+R)*S'*Q;          % optimality criterion
F = G*V;                          % optimality criterion

M = [G(:,1:2:2*Tp) G(:,2:2:2*Tp)];
M = M(1:2,:);
N = F(1:2,:);
%----- BUFFER system computation
clear Ab Bb Cb Db Z
on = ones(1,Tp-1);
Ab = diag(on,1);
Bb(Tp,1) = 1;
Cb=eye(Tp);
Db=zeros(Tp,1);
%----- Z matrix for the input signal display
Z=zeros(2,2*Tp);
Z(1,1)=1;
Z(2,Tp+1)=1;
```

We have chosen the receding horizon length to be equal to $T_p = 150$ and the cost matrices:

$$Q = 40 \cdot I \qquad R = I$$

where I is an identity matrix with appropriate size.

We substitute the computed matrices into the Simulink scheme Fig. 5.15, the interesting fact to notice is that there are two identical buffers. Their role is to slow down the input signal according to the prediction horizon and to provide the information about the signal to the controller.

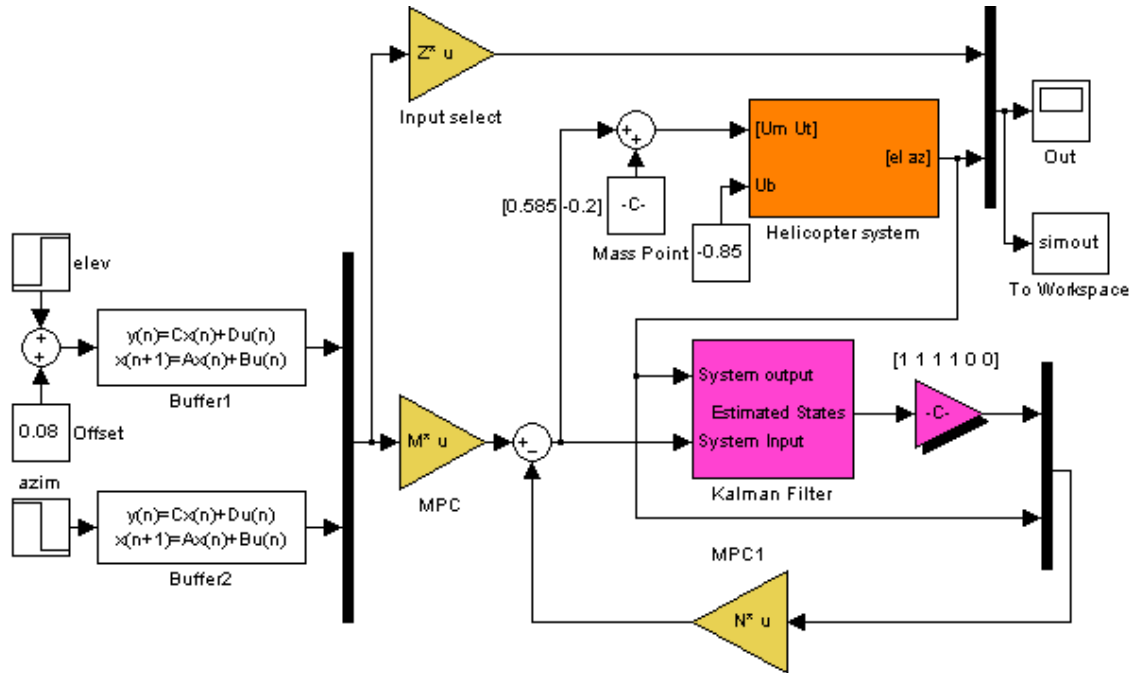


Figure 5.15: The Simulink scheme for the MPC

The matrix Z selects the signal that arrives to both inputs at each instant of time k .

The Fig. 5.16 shows the step responses of the closed loop system with coupling.

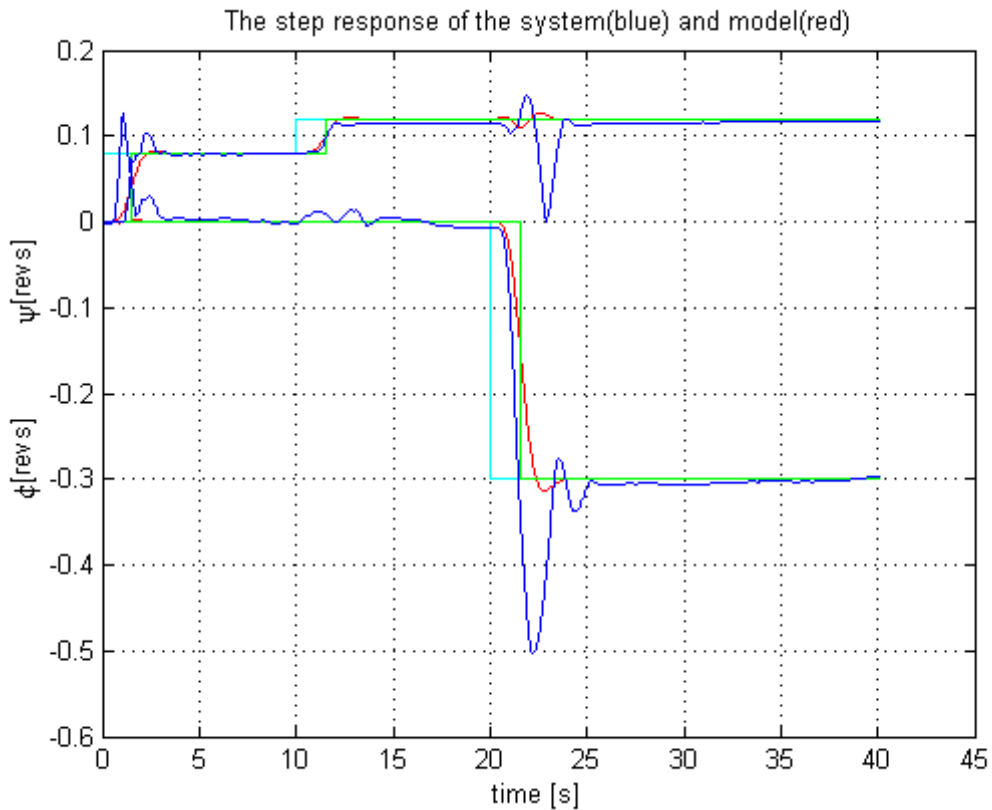


Figure 5.16: The comparison of the system and model step responses

As we expect the MPC is not causal, i.e.: it react on the change before it comes. The cyan color corresponds to the signal where MPC starts to 'see' the coming change. The green color corresponds to the input signal as it comes. We can also conclude that the measured step response is more oscillatory than the theoretically expected. This is due to big ratio of \mathbf{Q} and \mathbf{R} and uncertainties in the state estimation from the Kalman filter. The iterative optimization of constants will lead to the improvement of the transient responses.

The last thing to notice is the coupling. The coupling can be also improved by the cyclical optimization of constants.

Chapter 6

Virtual Reality

6.1 The design of VR objects

To design the Virtual Reality objects we used the V - Realm builder 2.0 with the available Object libraries Fig. 6.1.

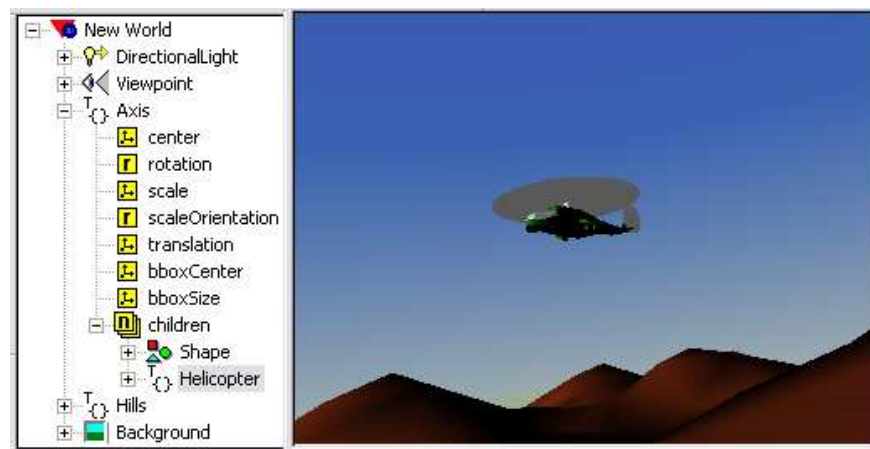


Figure 6.1: Virtual landscape and helicopter

The main problem to solve is the rotation of the virtual helicopter around two axes. To overcome the recomputation of rotational motion we construct the invisible object *Axis* e.g.: an ordinary cilinder with small diameter, and make the *helicopter* to be its child. Because all the transformations of the parent automatically transform to all its childs the helicoter will move (3D) and rotate in one axis through its parent object *Axis*. The rotation around the remaining axes is set directly to the helicopter.

The landscape - *Hills* and the background together with *DirectionalLight* and *View-Point* are static objects which enhance the scene.

6.2 Simulation

The interconnection of the VR sink block with the real system is shown on the Fig. 6.2.

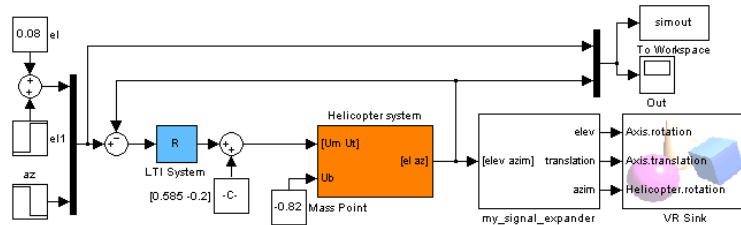


Figure 6.2: The interconnection of the VR with the Simulink scheme

The *signal expander* block is shown on the Fig. 6.3.

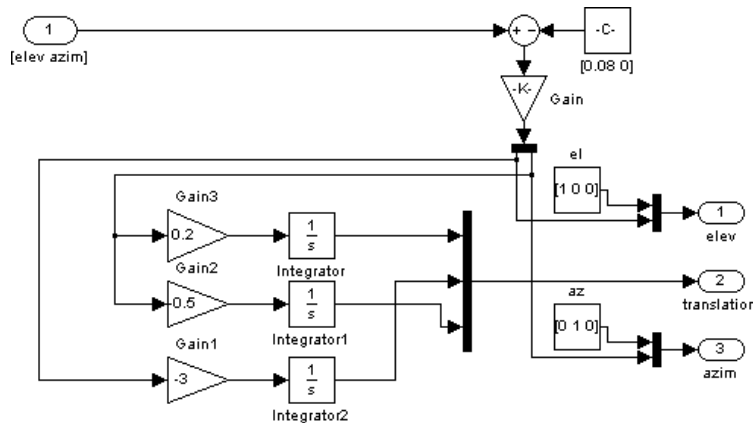


Figure 6.3: The internal interconnection of the signal expander

We used the PID controller to enhance the movement of the helicopter.

The parallel simulation of the virtual and real helicopter is available on the link:

<http://youtube.com/watch?v=EN6-aKYcfnk>

Chapter 7

Conclusion

The autopilots for the helicopters are already invented therefore the main goal of this work is to show new approach in the system identification and to apply the control algorithms (PD, PID, LQG and MPC) to the identified system.

The biggest problem through all the identification process is the decision making. The decisions taken during this phase are affecting the control synthesis. During the identification of the system we answered following questions:

- What is the shape of the signal for the system excitation (amplitude, duty cycles)?
- Which positions of the mass point are the best candidates for the working point selection?
- From which working point to start the system identification?
- In what units shall we keep the obtained results?
- How to process obtained data and how to extract the usefull information out of it?
- Which identification algorithm to trust under which conditions?

The highest cost (in terms of time consumption) has a decision to identify the dynamics of motors indirectly. Although the developed algorithms for the identification of motors *with and without holding* are mathematically elegant, this measurement is *reaction time of the examiner* sensitive and therefore not accurate.

During the control synthesis we sum up and compare all the obtained results. We prove the identification of all three working points to be accurate.

The working points are selected such that the H_∞ robust control design could have been applied. Unfortunately due to the lack of time the voluntary H_∞ control synthesis has not been realised.

Another voluntary control synthesis is MIMO MPC design. We manage to broaden the SISO MPC algorithm to the MIMO helicopter system. The further generalisation of the presented approach will lead to the general MIMO MPC design algorithm.

Thanks to inventive attitude of Mr. Vanek we managed to make a video presentation of the interconnected virtual with real helicopter flight.

The further use of this work is the demonstration of the impressive control results to new students who are taking the decision of their future specialisation.

Bibliography

JOHN, J. (1996), *Systémy a řízení*, Praha: Vydavatelství ČVUT.

FRANKLIN, G.F., POWEL, J.D. a EMAMI-NAEINI, A.; (2006), *Feedback Control of Dynamic Systems*, New Jersey: Prentice Hall

SKOGESTAD, S., POSTLETHWAITE, I.; (2003), *Multivariable Feedback Control*, West Sussex: John Wiley and Sons Ltd.

HAVLENA, V.; ŠTECHA, J. (2000), *Moderní teorie řízení*, Praha: Vydavatelství ČVUT.

ROUBAL, J., PEKAŘ, J., PACHNER, D. a HAVLENA, V.; (2005), *Moderní teorie řízení – Cvičení*, Praha: Vydavatelství ČVUT.

<http://www.humusoft.cz/models/ce150.htm>

<http://dce.felk.cvut.cz/roubal>

<http://youtube.com/watch?v=EN6-aKYcfnk>

Attachments A

The content of attached CD

The CD with source codes has been attached to this work.

Documentation : contains the source codes of this documentation written in \LaTeX .

Codes : contains commented Matlab codes that have been used for the system identification and control design.

Video : contains the video of the real time control of the helicopter.